Chapter 5

PROPERTIES OF IRRADIATED LBE AND Pb*

5.1 Introduction

Lead and LBE possess favourable properties as both a spallation neutron target material and as a coolant for ADS and reactor systems. For ADS applications, these properties include: 1) a high yield of about 28 n for LBE and 24 n for Pb per 1 GeV proton; 2) both melts have an extremely small neutron absorption cross-section; (3) a small scattering cross-section [Gudowski, 2000]. As a coolant, lead and LBE possess: 1) high boiling points; 2) high heat capacities; (3) inert behaviour with respect to reaction with water.

For safe operation and post-irradiation handling of LBE and Pb it is necessary to know the nuclides generated during irradiation. Some of these nuclides are volatile, hazardous and rather long-lived. Their behaviour within the system is strongly influenced by the environment including the oxygen content and temperature. If volatiles are produced, their release rates under specific conditions must be evaluated. The release of volatiles may be prevented by the application of a suitable absorber.

Protons of 600 MeV energy induce spallation reactions in heavy materials such as Pb and Bi. These reactions generate direct spallation products, consisting of nuclei with masses close to that of the target nuclei. At the high energies involved multiple inelastic reactions are possible. Therefore, one must expect a large number of isotopes as products. For instance, reactions on Pb generate Hg isotopes roughly from ^{180}Hg to ^{206}Hg.

Similarly, reactions of protons on Bi generate Po isotopes up to ^{209}Po. ^{210}Po is generated by neutron capture on ^{209}Bi, and subsequent β decay of the compound nucleus ^{210}Bi. Neutron capture of course exist for all the isotopes with a high capture cross-section, not only for ^{209}Bi. Another source of Po in pure Pb systems is the production of ^{209}Pb from ^{208}Pb followed by β^- decay to ^{209}Bi. Po production then proceeds as described above by neutron capture to form ^{210}Bi and β^- decay. In critical systems such as the Lead Fast Reactor (LFR), Po production is a serious issue when LBE is the coolant due to the direct production from Bi. However, it is also a concern in Pb-cooled systems due to the multi-step reaction beginning with ^{208}Pb as described above. Other direct products of high energy reactions include light particles, such as ^{4}He, hydrogen and tritium. Also fissions are induced by high energy protons as well as thermal and fast neutrons. Fission products are lighter elements, and include for instance I, Ar, Kr, Xe and so on. In particular, halogen containing species, iodine compounds for example, will also be important since they may be volatile.

The influence of protons with energies of 590 MeV [Pitcher, 2002], [Foucher, 2002], [Zanini, 2005] and 72 MeV [Foucher, 2002] to LBE were calculated with Monte Carlo programs and it was shown that the full spectrum of isotopes (light, medium and heavy elements) are generated during the

---

* *Chapter lead: Heike Glasbrenner (PSI, Switzerland). For additional contributors, please see the List of Contributors included at the end of this work.*

irradiation process in an ADS system. Since the most hazardous isotopes (Po, Hg) are produced directly from the major components in LBE, a detailed specification that includes the concentrations of contaminants has not been specified for nuclear systems.

In the following chapter theoretical considerations concerning the formation and behaviour of polonium and iodine are discussed. Thermodynamic properties of polonium are derived in an extrapolative manner from its group homologous. In a similar way, thermodynamic properties of some polonium compounds important for LBE systems are derived. The interaction of polonium with metals in the condensed phase is treated using the semi-empirical Miedema model [de Boer, 1988]. Some results achieved by irradiation experiments of LBE and subsequent investigation are presented. Selective isotopes have been generated in LBE and their evaporation and absorption behaviour investigated. The release of volatiles from a liquid LBE target was studied on-line in an experiment at CERN-ISOLDE. These results are also presented and discussed.

5.2 Theoretical considerations

5.2.1 Evaporation characteristics of polonium

Thermodynamic constants that describe the evaporation processes of polonium are summarised and critically discussed by Eichler [Eichler, 2002]. Additionally, systematic changes of the properties of the chalcogenes are analysed, empirical correlations are proposed and cyclic processes are balanced. Accordingly, the existing values of entropies for polonium are acceptable. Questionable, however, are those values of enthalpies, which have been deduced from results of the experimental investigations of the vapour pressure temperature dependency, of the melting point, and of the boiling temperatures. Technical difficulties and possible error sources of the measurements resulting from the radioactive decay properties of ^{210}Po are discussed. Using extrapolative standard enthalpies and entropies as well as their temperature dependency, shown in Tables 5.2.1-5.2.3 [Eichler, 2002], empirical correlations for the equilibrium partial pressure of monomeric and dimeric polonium above the pure condensed phase and the equilibrium constant of the dimerisation reaction in the gas phase are as follows:

$$\log p(Po(g))/Pa = (11.797 \pm 0.024) - (9883.4 \pm 9.5)/T;\ T = 298\text{-}600\ K \quad (5.1)$$

$$\log p(Po(g))/Pa = (10.661 \pm 0.057) - (9328.4 \pm 4.9)/T;\ T = 500\text{-}1300\ K \quad (5.2)$$

$$\log p(Po_2(g))/Pa = (13.698 \pm 0.049) - (8592.3 \pm 19.6)/T;\ T = 298\text{-}600\ K \quad (5.3)$$

$$\log p(Po_2(g))/Pa = (11.424 \pm 0.124) - (7584.1 \pm 98.1)/T;\ T = 500\text{-}1300\ K \quad (5.4)$$

$$\log K_d = (-4.895 \pm 0.012) + (11071 \pm 6)/T \quad (5.5)$$

with p as pressure in Pa, T the temperature in K and K_d the equilibrium constant of the dimerisation reaction $K_d = (Po_2(g))/p(Po(g))^2$.

Figure 5.2.1 shows plots of the above empirical correlations [Eichler, 2002] together with experimental data determined by [Abakumov, 1974], [Brooks, 1955], [Ausländer, 1955] and [Beamer, 1946]. According to the extrapolations, the dominant gas phase species of polonium in the entire temperature range between 298 and 1300 K should be dimeric polonium. Experimental evidence on the actual gas phase species present, or the ratio of monoatomic and diatomic polonium in the gas phase, is not available. All experimental vapour pressure measurements were performed using ^{210}Po. These measurements are inevitably influenced by effects such as self heating of ^{210}Po by decay heat and sputtering, thus giving rise to erroneous results especially at low temperatures. Hence, extrapolated

"latent heats" of the volatilisation processes are clearly larger compared to literature data. Especially in the temperature range of solid polonium the calculated vapour pressure curve shifts significantly to lower values, whereas the boiling point was almost reproduced by the calculation. For a critical discussion of the literature data see [Eichler, 2002].

Table 5.2.1. Temperature dependent standard entropies ($Jmol^{-1}K^{-1}$) and standard enthalpies ($kJmol^{-1}$) of polonium (selected extrapolation results) [Eichler, 2002]

T (K)	$S_TPo(g)$	$H_TPo(g)$	$S_TPo(l)$	$H_TPo(l)$	$S_TPo(s)$	$H_TPo(s)$	$S_TPo_2(g)$	$H_TPo_2(g)$
298	187.13	188.9	–	–	55.20	0.00	282.24	166.2
300	187.28	188.9	–	–	55.36	0.05	282.49	166.3
400	193.20	190.9	–	–	66.16	2.74	294.22	170.4
500	197.89	192.9	96.13	16.88	69.68	5.75	303.40	174.5
600	201.75	194.9	99.97	20.38	75.39	8.94	310.98	178.7
700	205.06	197.0	104.08	24.51	80.54	12.36	317.47	182.9
800	207.36	199.1	107.94	28.36	–	–	323.15	187.1
900	210.52	201.3	111.94	32.06	–	–	328.22	191.4
1000	212.89	203.4	115.20	35.83	–	–	332.80	195.8
1100	215.02	205.6	118.20	39.60	–	–	337.00	200.2
1200	217.00	207.9	120.85	43.37	–	–	340.88	204.7
1300	218.83	210.1	123.22	46.37	–	–	344.49	209.2

Table 5.2.2. Temperature dependence of standard entropy of polonium (extrapolation)

Standard entropy: $S^0_T\,(Jmol^{-1}K^{-1}) = A + BT + CT^2 + DT^3$ [Eichler 2002]

	A	B	C	D
$S_TPo(g) \pm \Delta$	164.30495	0.0947	$-6.51757*10^{-5}$	$1.89789*10^{-8}$
298-1300 K	0.708	0.0033	$4.60499*10^{-6}$	$1.94088*10^{-9}$
$S_TPo(l) \pm \Delta$	78.25652	0.02762	$2.25857*10^{-5}$	$-1.32887*10^{-8}$
500-1300 K	2.40963	0.00876	$1.01247*10^{-5}$	$3.73800*10^{-9}$
$S_TPo(s) \pm \Delta$	21.06849	0.14888	$-1.33057*10^{-4}$	$5.96463*10^{-8}$
298-700 K	0.51653	0.00343	$7.21707*10^{-6}$	$4.83576*10^{-9}$
$S_TPo_2(g) \pm \Delta$	237.11031	0.18734	$-1.29537*10^{-4}$	$3.77809*10^{-8}$
298-1300 K	1.31574	0.00618	$8.55737*10^{-6}$	$3.6061*10^{-9}$

Table 5.2.3. Temperature dependence of standard enthalpy of polonium (extrapolation)

Standard enthalpy: $\Delta H^0_T\,(kJmol^{-1}) = A + BT + CT^2 + DT^3$ [Eichler 2002]

	A	B	C	D
$H_TPo(g) \pm \Delta$	183.22359	0.01829	$2.15156*10^{-6}$	$-2.33463*10^{-10}$
298-1300 K	0.01493	$7.01599*10^{-5}$	$9.70807*10^{-8}$	$4.09105*10^{-11}$
$H_TPo(l) \pm \Delta$	2.0991	0.02024	$2.33896*10^{-5}$	$-9.77999*10^{-9}$
500-1300 K	1.37678	0.0055	$6.82892*10^{-6}$	$2.66605*10^{-9}$
$H_TPo(s) \pm \Delta$	-5.97236	0.014	$2.23597*10^{-5}$	$-7.07494*10^{-9}$
298-700 K	0.38876	0.00258	$5.43228*10^{-6}$	$3.63987*10^{-9}$
$H_TPo_2(g) \pm \Delta$	154.42684	0.03892	$2.44905*10^{-6}$	$1.74859*10^{-12}$
298-1300 K	0.07976	$3.7491*10^{-4}$	$5.18766*10^{-7}$	$2.18611*10^{-10}$

Figure 5.2.1. Logarithm of the vapour pressure of polonium (bar) as a function of reciprocal temperature (extrapolation and experimental results)

The solid-liquid transition temperature is indicated by an arrow

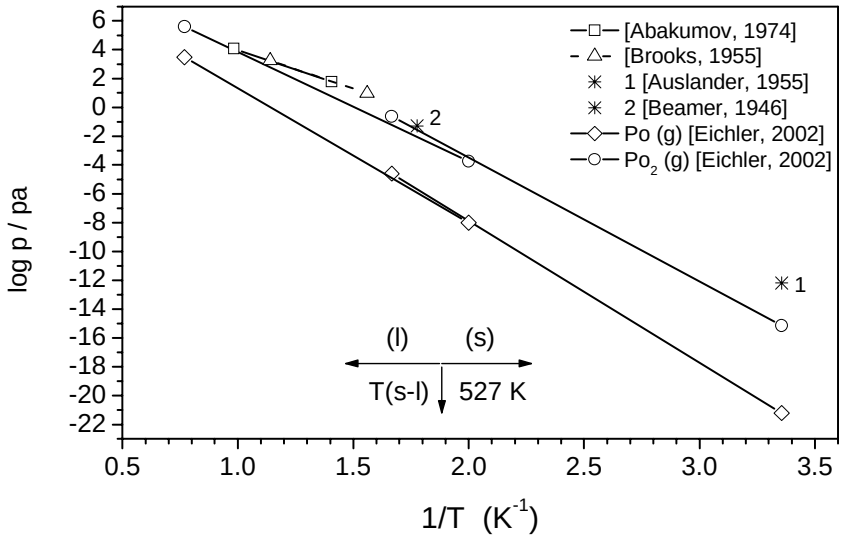

The results of the extrapolation for the standard enthalpy of the gaseous monomeric polonium and the dimerisation enthalpy are:

$$\Delta H^0_{298}\text{Po (g)} = 188.9 \text{ kJ/mol and } \Delta H^0_{298}\text{(form) Po}_2\text{ (g)} = 211.5 \text{ kJ/mol} \quad (5.6)$$

The preferred evaporation of pure polonium in the dimeric state requires new interpretations of the thermodynamic relations of polonium in mixed phases (activity coefficients), if the experimental conditions exclude a formation of the dimers due to low concentrations.

The thermodynamic data derived by extrapolation [Eichler, 2002], while not highly accurate, at least represent a consistent set of data. To acquire more reliable data, that are essential for the prediction of polonium behaviour in a technical system, experimental thermodynamic studies using polonium isotopes which are less prone to radiation effects, such as ^{209}Po, are definitely necessary.

5.2.2 Volatilisation pathways of polonium

An analysis of the literature data for the thermochemical constants of polonium shows substantial deviations in the relations of these constants among each other, as well as in the expected trends of these constants within the chalcogen group [Eichler, 2002]. This fact considerably complicates the assessment of possible release paths for polonium from a lead-bismuth spallation target or critical system and reduces the reliability of predictions and estimations.

For elemental polonium, a coherent set of thermodynamic data was extrapolated and critically discussed in [Eichler, 2002] (see Section 5.2.1). For polonium compounds, almost no experimental thermodynamic data are available. Therefore, as a first step, a coherent set of thermodynamic data for polonium hydride, lead polonide and polonium dioxide was derived using extrapolative procedures by Eichler, *et al.* [Eichler, 2004a]. Using these data, the equilibrium constants of formation, dissociation and evaporation reactions were calculated. Furthermore, equilibrium constants for the reactions of lead polonide and polonium dioxide with hydrogen, water vapour as well as with lead and bismuth were

evaluated. It has to be pointed out that such extrapolations do not give results of high accuracy. Precise measurements of thermodynamic data of polonium compounds that would be required for engineering purposes are scarce. Thus, the extrapolated data can be considered as best available estimates. Detailed experimental studies of the discussed systems, preferably using ^{209}Po are strongly recommended.

Based on the results of extrapolations, possible volatilisation processes are evaluated. From this assessment, volatilisation of polonium most likely occurs in form of diatomic polonium molecules or as diatomic intermetallic molecules. Rates for the release of radioactivity and their temperature dependency have been calculated. The main results of this study are summarised in the following section.

For the entropy of polonium hydride the following temperature function is recommended:

$$S_T H_2Po(g) = (206.07678 \pm 1.41) + (0.12098 \pm 0.00437)*T - (3.73042*10^{-5} \pm 2.97*10^{-6}) *T^2 \quad (5.7)$$

Entropy values for polonium hydride together with those of polonium and hydrogen are compiled in Table 5.2.4.

Calculated entropy of formation values for polonium hydride are compiled in Table 5.2.5 for the six different formation reactions given below [Eqs. (5.8) to (5.13)]. The corresponding enthalpy and Gibbs free energy values are given in Tables 5.2.6 and 5.2.7.

$$Po\ (cond) + H_2\ (g) <===> H_2Po\ (g) \quad (5.8)$$

$$Po\ (g) + H_2\ (g) <===> H_2Po\ (g) \quad (5.9)$$

$$0.5\ Po_2\ (g) + H_2\ (g) <===> H_2Po\ (g) \quad (5.10)$$

$$Po\ (cond) + 2H\ (g) <===> H_2Po\ (g) \quad (5.11)$$

$$Po\ (g) + 2\ H\ (g) <===> H_2Po\ (g) \quad (5.12)$$

$$0.5\ Po_2\ (g) + 2\ H\ (g) <===> H_2Po\ (g) \quad (5.13)$$

Table 5.2.4. Standard entropies of gaseous polonium hydride, dimeric and monoatomic gaseous polonium and hydrogen

T (K)	$S^0_T H_2Po$ (g) ($Jmol^{-1}K^{-1}$)	S^0_T Po(s;l) ($Jmol^{-1}K^{-1}$) [Eichler, 2002]	S_T Po (g) ($Jmol^{-1}K^{-1}$) [Eichler, 2002]	S_T Po_2 (g) ($Jmol^{-1}K^{-1}$) [Eichler, 2002]	$S^0_T H_2$ (g) ($Jmol^{-1}K^{-1}$) [Barin, 1995]	S_T H (g) ($Jmol^{-1}K^{-1}$) [Barin, 1995]
298	238.13	55.20	187.13	282.24	130.68	114.716
300	238.35	55.36	187.28	282.49	130.86	114.845
400	249.49	63.16	193.20	294.22	139.22	120.824
500	258.09	69.68	197.89	303.40	145.74	125.463
600	265.76	99.97	201.75	310.98	151.08	29.252
700	272.51	104.08	205.06	317.47	155.61	132.457
800	278.56	107.94	208.00	323.15	159.55	135.232
900	284.07	111.94	210.52	328.22	163.05	137.680
1000	289.15	115.20	212.88	332.8	166.22	139.870
1100	293.88	118.2	215.02	337.00	169.11	141.851
1200	298.31	120.85	216.99	340.88	171.79	143.660

Table 5.2.5. Entropy of polonium hydride formation for different reactions

T (K)	$\Delta S^0_{T,form}$ $H_2Po(g)$ ($Jmol^{-1}K^{-1}$) Eq. (5.8)	$\Delta S_{T,form}$ $H_2Po(g)$ ($Jmol^{-1}K^{-1}$) Eq. (5.9)	$\Delta S_{T,form}$ $H_2Po(g)$ ($Jmol^{-1}K^{-1}$) Eq. (5.10)	$\Delta S_{T,form}$ $H_2Po(g)$ ($Jmol^{-1}K^{-1}$) Eq. (5.11)	$\Delta S_{T,form}$ $H_2Po(g)$ ($Jmol^{-1}K^{-1}$) Eq. (5.12)	$\Delta S_{T,form}$ $H_2Po(g)$ ($Jmol^{-1}K^{-1}$) Eq. (5.13)
298	52.25	-79.68	-33.67	-46.50	-178.43	-132.42
300	52.13	-79.79	-33.76	-46.70	-178.62	-132.59
400	47.11	-82.93	-36.84	-55.32	-185.36	-139.27
500	42.67	-85.54	-39.35	-62.52	-190.73	-144.54
600	14.71	-87.07	-40.81	-92.71	-194.49	-148.23
700	12.82	-88.16	-41.84	-96.48	-197.46	-151.14
800	11.07	-88.99	-42.09	-99.84	-199.01	-153.48
900	9.08	-89.5	-42.57	-103.23	-201.81	-155.40
1000	7.73	-89.95	-43.47	-105.79	-203.47	-156.99
1100	6.57	-90.25	-43.73	-108.02	-204.84	-158.32
1200	5.67	-90.47	-43.92	-109.86	-206.00	-159.45

Table 5.2.6. Standard formation enthalpy for polonium hydride and enthalpies for its formation from the elements in different states [Reactions (5.8) to (5.13)]

T (K)	$\Delta H^o_{T,form}H_2Po(g)$ ($kJmol^{-1}$) Eq. (5.8)	$\Delta H_{T,form}H_2Po(g)$ ($kJmol^{-1}$) Eq. (5.9)	$\Delta H_{T,form}H_2Po(g)$ ($kJmol^{-1}$) Eq. (5.10)	$\Delta H_{T,form}H_2Po(g)$ ($kJmol^{-1}$) Eq. (5.11)	$\Delta H_{T,form}H_2Po$ (g) ($kJmol^{-1}$) Eq. (5.12)	$\Delta H_{T,form}H_2Po$ (g) ($kJmol^{-1}$) Eq. (5.13)
298	163.0	-25.9	79.9	-273.0	-461.9	-356.1
300	165.9	-22.9	82.8	-270.1	-459.0	-353.2
400	164.9	-23.2	82.5	-272.3	-460.5	-354.8
500	166.2	-20.9	84.7	-272.2	-459.4	-353.7
600	152.0	-22.6	83.0	-187.8	-462.3	-356.8
700	149.1	-23.4	82.2	-291.8	-464.3	-358.8
800	146.7	-24.0	81.5	-295.4	-466.2	-360.6
900	144.6	-24.6	81.0	-298.7	-468.0	-362.4
1000	141.9	-25.7	79.8	-302.6	-470.2	-364.7
1100	140.4	-25.6	79.9	-305.2	-471.2	-365.7
1200	137.6	-27.0	78.6	-309.1	-473.7	-368.1

Table 5.2.7. Temperature dependency of Gibbs free energy values for polonium hydride formation [Eqs. (5.8) to (5.13)]

T (K)	$\Delta G^o_{T,form}H_2Po(g)$ ($kJmol^{-1}$) Eq. (5.8)	$\Delta G_{T,form}H_2Po(g)$ ($kJmol^{-1}$) Eq. (5.9)	$\Delta G_{T,form}H_2Po(g)$ ($kJmol^{-1}$) Eq. (5.10)	$\Delta G_{T,form}H_2Po(g)$ ($kJmol^{-1}$) Eq. (5.11)	$\Delta G_{T,form}H_2Po(g)$ ($kJmol^{-1}$) Eq. (5.12)	$\Delta G_{T,form}H_2Po(g)$ ($kJmol^{-1}$) Eq. (5.13)
298	147.4	-2.2	89.9	-259.2	-408.8	-316.7
300	150.0	1.0	92.9	-256.2	-405.5	-313.5
400	146.1	10.0	97.2	-254.5	-390.6	-303.3
500	144.9	21.9	104.4	-249.4	-372.4	-289.8
600	143.1	29.7	107.5	-244.7	-358.2	-280.4
700	140.1	38.3	111.5	-241.0	-342.8	-269.7
800	137.9	47.2	115.6	-236.4	-327.1	-258.7
900	136.4	55.9	119.7	-230.9	-311.4	-247.5
1000	134.1	64.2	123.3	-226.0	-295.9	-236.9
1100	133.2	73.7	128.0	-219.7	-279.2	-224.9
1200	130.8	81.6	131.3	-214.8	-263.9	-214.3

The following temperature functions have been derived from Tables 5.2.8 and 5.2.9 for the entropy of gaseous and solid lead polonide [Eichler, 2004a]:

$$S_T \text{ PbPo (g)} = 233.2798 + 0.19892\ T - 1.5756*10^{-4}\ T^2 + 5.19651*10^{-8}\ T^3 \quad (5.14)$$

$$S_T \text{ PbPo (s)} = 53.19976 + 0.27136\ T - 2.1165*10^{-4}\ T^2 + 7.16652*10^{-8}\ T^3 \quad (5.15)$$

This results in the following relation for the entropy of sublimation:

$$\Delta S_T(\text{subl}) \text{ PbPo} = 180.08004 - 0.07244T + 5.40902*10^{-5}T^2 - 1.97001*10^{-8}\ T^3 \quad (5.16)$$

Entropy and enthalpy values for PbPo are compiled in Tables 5.2.8 and 5.2.9 together with the entropy of sublimation and the entropies of formation of gaseous and solid PbPo from the elements in their standard state at the given temperature. Gibbs free energy values for these formation reactions as well as the sublimation reaction are listed in Table 5.2.10 together with the corresponding equilibrium constants or vapour pressures, respectively.

Extrapolated entropy values for polonium dioxide are given in Table 5.2.11 together with its entropy of sublimation and formation.

Enthalpy data have been extrapolated for the formation of gaseous and solid polonium dioxide from the gaseous monoatomic elements, i.e. oxygen and polonium. These values are compiled in Table 5.2.12 together with the resulting values for enthalpy of sublimation and vapour pressure. The derived enthalpy values should be regarded cautiously because they are based on rather few literature data for chalcogen dioxides (SeO_2 and TeO_2) and the chemical bonding in these compounds (polar covalent) differs substantially from the bonding in PoO_2 (partially ionic).

Table 5.2.8. Extrapolated entropy values of gaseous and solid lead polonide, sublimation entropy of PbPo and entropies for the formation of gaseous and solid PbPo from the elements in their standard state [Eichler, 2004a]

T (K)	S_T (g) ($Jmol^{-1}K^{-1}$)	S_T (s) ($Jmol^{-1}K^{-1}$)	ΔS (subl) ($Jmol^{-1}K^{-1}$)	ΔS (form) PbPo (g) ($Jmol^{-1}K^{-1}$)	ΔS(form) PbPo (s) ($Jmol^{-1}K^{-1}$)
298	285.46	122.61	162.854	159.919	-2.941
300	285.57	122.92	162.651	159.722	-2.918
400	295.25	137.87	157.383	152.441	-6.139
500	304.85	149.72	155.130	150.807	-3.720
600	311.69	159.62	152.067	122.927	-29.143
700	317.46	168.19	149.273	112.128	-37.115
800	322.45	175.77	146.683	108.771	-37.911
900	326.84	182.60	144.245	106.330	-37.910
1000	330.77	188.84	141.930	103.989	-37.940
1100	334.31	194.60	139.715	101.814	-37.900

Table 5.2.9. Extrapolated enthalpy values of gaseous and solid lead polonide, sublimation enthalpy of PbPo and enthalpies for the formation of gaseous and solid PbPo from the elements in their standard state [Eichler, 2004a]

T (K)	H_T PbPo (g) ($kJmol^{-1}$)	H_T PbPo (s) ($kJmol^{-1}$)	ΔH_T (subl) PbPo ($kJmol^{-1}$)	ΔH_T(form) PbPo (g) ($kJmol^{-1}$)	ΔH_T (form) PbPo (s) ($kJmol^{-1}$)
298	184.2	-35.43	219.6	184.20	-35.43
300	183.7	-35.25	218.9	183.55	-35.36
400	186.6	-30.14	216.7	181.07	-35.66
500	190.4	-25.26	215.7	179.05	-36.60
600	195.1	-18.97	214.1	166.20	-47.84
700	199.7	-12.61	212.3	158.90	-53.43
800	204.0	-6.47	210.5	156.31	-54.16
900	208.3	-0.14	208.5	153.96	-54.51
1000	212.4	5.93	206.5	151.34	-55.17
1100	217.1	12.13	204.9	149.26	-55.66

Table 5.2.10. Gibbs free energy for the formation and sublimation reactions of lead polonide and the corresponding equilibrium constants [Eichler, 2004a]

T (K)	ΔG (form) PbPo (s) ($kJmol^{-1}$)	lg K_{form}	ΔG (form) PbPo (g) ($kJmol^{-1}$)	lg K_{form}	ΔG (subl) PbPo (s) ($kJmol^{-1}$)	lg p_{PbPo} p/(bar)
298	-34.55	6.055	136.54	-23.931	171.09	-29.986
300	-34.48	6.003	135.63	-23.613	170.12	-29.616
400	-33.21	4.336	120.094	-15.680	153.30	-20.017
500	-33.744	3.629	103.65	-10.826	138.39	-14.455
600	-30.35	2.642	92.44	-8.047	122.80	-10.689
700	-27.45	2.048	80.41	-5.999	107.86	-8.047
800	-22.83	1.490	69.29	-4.524	92.12	-6.014
900	-20.39	1.183	58.26	-3.381	78.654	-4.564
1000	-17.23	0.899	47.35	-2.473	64.58	-3.373
1100	-13.97	0.663	37.26	-1.769	51.23	-2.433

Table 5.2.11. Temperature dependence of the entropy of polonium dioxide

Sublimation entropy of PoO_2 and entropy of formation for gaseous and solid PoO_2 [Eichler, 2004a]

T (K)	S_T PoO_2 (g) ($Jmol^{-1}K^{-1}$)	S_T PoO_2 (s) ($Jmol^{-1}K^{-1}$)	ΔS_T (subl) PoO_2 ($Jmol^{-1}K^{-1}$)	ΔS_T (form) PoO_2 (g) ($Jmol^{-1}K^{-1}$)	ΔS_T (form) PoO_2 (s) ($Jmol^{-1}K^{-1}$)
298	286.29	82.41	203.89	25.945	-177.94
300	286.57	82.84	203.73	25.878	-177.85
400	300.47	103.07	197.40	23.439	-173.96
500	312.20	118.45	193.76	21.83	-171.93
600	322.09	130.60	191.50	-4.327	-195.82
700	330.56	141.62	188.94	-4.984	-193.93
800	338.02	152.19	185.84	-5.839	-191.68
900	344.63	162.96	181.67	-7.238	-188.91
1000	350.59	174.38	176.21	-8.189	-184.40
1100	356.01	185.11	170.90	-9.108	-180.01

Table 5.2.12. Temperature dependence of the enthalpy of polonium dioxide formation from gaseous mono-atomic elements. Sublimation enthalpy of PoO_2 and its vapour pressure.

T (K)	ΔH^*_T (form) PoO_2 (g) ($kJmol^{-1}$)	ΔH^*_T (form) PoO_2 (s) ($kJmol^{-1}$)	ΔH_T (subl) PoO_2 ($kJmol^{-1}$)	log p_{PoO2} (bar)
298	-690.6	-1054.2	363.7	-53.0847
300	-690.5	-1054.1	363.6	-52.6527
400	-684.2	-1053.8	369.6	-37.9440
500	-685.2	-1053.2	368.0	-28.3177
600	-688.5	-1052.4	364.0	-21.6786
700	-692.6	-1051.1	358.5	-16.8783
800	-697.3	-1050.6	353.3	-13.3618
900	-699.0	-1049.9	350.9	-10.8769
1000	-702.0	-1049.0	347.0	- 8.9211

Equilibrium constants for the following reactions were calculated from entropy and enthalpy values:

Formation reaction: $Po\,(cond) + O_2\,(g) <==> PoO_2\,(s)$ (5.17)

Dissociation: $PoO_2\,(cond) <==> Po\,(g) + O_2\,(g)$ (5.18)

$2\,PoO_2\,(cond) <==> Po_2\,(g) + 2\,O_2$ (5.19)

Reduction with hydrogen: $PoO_2\,(s) + 2\,H_2\,(g) <==> Po\,(cond) + 2H_2O\,(g)$ (5.20)

Reduction with lead: $PoO_2\,(s) + 2\,Pb\,(cond) <==> Po\,(cond) + 2PbO\,(s)$ (5.21)

Reduction with bismuth: $3PoO_2\,(s) + 4\,Bi\,(cond) <==> 3Po\,(cond) + 2\,Bi_2O_3\,(s)$ (5.22)

The calculated equilibrium constants are shown in Table 5.2.13. The calculated values generally reflect the actually observed chemical behaviour of polonium dioxide [Gmelin, 1990]. Nevertheless, it is possible that the enthalpy of formation of solid PoO_2 is overestimated. The dissociative volatilisation of PoO_2 observed in vacuum as observed opposed to the congruent sublimation of PoO_2 in the presence of oxygen can not be explained by these data. However, it remains to be clarified to what extent radiolysis effects may play an additional role in the volatilisation process.

Table 5.2.13. Equilibrium constants of formation, dissociation and some redox reactions of polonium dioxide

T (K)	lgK Eq. (5.17)	lgK Eq. (5.18)	lgK Eq. (5.19)	lgK Eq. (5.20)	lgK Eq. (5.21)	lgK Eq. (5.22)
298	55.0186	-91.9491	-151.6368	25.0874	11.0814	7.8522
300	54.5810	-91.2891	-150.5667	25.0030	11.0490	7.9350
400	38.6900	-67.4778	-113.3430	19.8000	7.9740	5.7201
500	29.1570	-53.2184	-89.1903	16.6250	6.1590	4.5029
600	22.4892	-43.7087	-73.8741	14.7848	5.2828	4.2965
700	17.8969	-36.9287	-62.9461	13.2791	4.3851	3.4093
800	14.5364	-31.9854	-54.9718	12.0496	3.6396	2.5329
900	11.9543	-28.1527	-48.8971	11.0517	3.0397	1.7910
1000	10.0102	-25.1956	-44.2274	10.1218	2.4498	0.8614
1100	8.4682	-22.8200	-40.4811	9.3079	1.9299	0.2755

5.2.3 Evaluation of thermochemical data for binary polonium containing systems by means of the semi-empirical Miedema model

Thermochemical data for binary metal-polonium systems have been calculated using the semi-empirical Miedema model [Boer, 1988]. The Miedema model is a semi-empirical model for the calculation of enthalpies of formation and enthalpies of mixing in solid and liquid binary metal systems. The element specific constants involved in the calculations are derived from properties of the elements and subsequently adjusted to give the best possible fit to known experimental enthalpy data. In spite of this empirical character, the physical significance of the parameters is obvious. Therefore, the classification of the model as semi-empirical is justified. Through the process of adjustment of parameters to experimental data, the model incorporates the complete knowledge of enthalpy effects in binary alloy systems.

The Miedema model is a cellular model. The principles and applications of the model are discussed in detail in [Boer, 1988]. Within the framework of the model, an alloy is thought to be built up from atomic cells of the constituent elements, each with a defined atomic volume. When cells of two different elements A and B are brought into contact to form an alloy (Figure 5.2.2), there will be discontinuities of the electron density n_{ws} at the boundaries of their (Wigner-Seitz) atomic cells. To eliminate these discontinuities, a rearrangement of the electron distribution within the atomic cell is required. This involves a transfer of electrons into higher energy levels and thus leads to a positive contribution to the enthalpy of formation or mixing. This positive contribution is found to be proportional to the squared differences in cube root of the electron densities, $n_{ws}^{1/3}$, of the constituent elements in the state of a bulk metal.

Values for n_{ws} for transition metals have been derived from experimental data of the bulk modulus and molar volume. For non-transition metals, a superposition of the charge densities of free atoms placed at individual lattice points was found to be an acceptable approximation for n_{ws} [Boer, 1988].

Figure 5.2.2. Schematic cellular model of the formation of an alloy AB from two pure metals A and B [Boer, 1988]

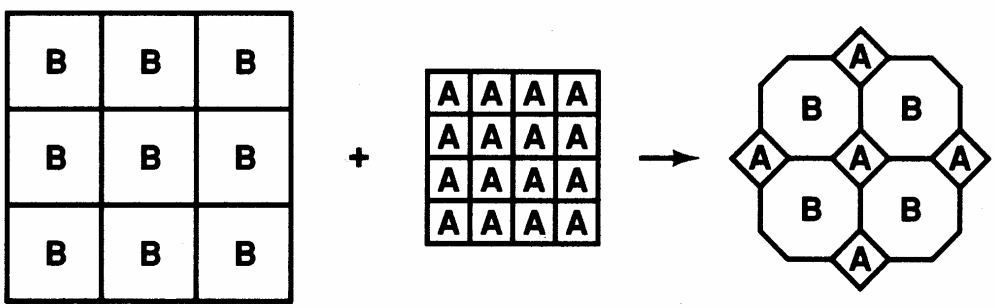

A negative contribution to the enthalpies of formation or mixing, which is stabilising with respect to the constituent elements, arises from the equalisation of the chemical potential of the electronic charge, Φ*, between dissimilar atomic cells. Φ*, also called Miedema-electronegativity, was originally derived from the work functions of the pure metals and afterwards adjusted using available experimental data of enthalpies of formation. This contribution is proportional to the square of the differences of Miedema-Electronegativities of the constituent elements. Thus, for the interfacial enthalpy effect between neighbouring atomic cells we arrive at the following proportionality:

$$\Delta H^{interface} \propto -P(\Delta\Phi^*)^2+Q(\Delta n_{ws}^{1/3})^2 \qquad (5.23)$$

where $\Delta H^{interface}$ is the enthalpy effect at the interface between dissimilar atomic cells, P and Q are the empirical constants for specific combinations of metals, tabulated in [Boer, 1988], $\Delta\Phi^*$ is the difference of Miedema electronegativities of the constituents and Δn_{ws} is the difference of electron densities at the Wigner-Seitz cell boundary of the constituents.

A quantification of this relation, as discussed extensively in [Boer, 1988], involves the introduction of several other group and element specific constants and leads to the following equations for the enthalpies of formation of ordered solid alloys $A_{x_A}B_{x_B}$:

A quantification of this relation, as discussed extensively in [Boer, 1988], involves the introduction of several other group and element specific constants and leads to the following equations for the enthalpies of formation of ordered solid alloys $A_{x_A}B_{x_B}$:

$$\Delta H^{f}\,A_{x_A}B_{x_B}(s) = x_A\,V_{A,\,alloy}^{2/3}\;f_B^A\;[-P(\Delta\Phi^*)^2+Q(\Delta n_{WS}^{1/3})^2-R_m]/ \\ [(n_{WS}A)^{-1/3}+(n_{WS}B)^{-1/3}]+x_A\,\Delta H^{trans}\,A+x_B\,\Delta H^{trans}\,B \qquad (5.24)$$

and for the partial molar enthalpies of solution at infinite dilution in solid (liquid) mixtures of A and B:

$$\Delta\overline{H}^{solv}{}_{A\text{ in }B}(l): = 2\,V_{A,\,alloy}^{2/3}[-P(\Delta\Phi^*)^2+Q(\Delta n_{WS}^{1/3})^2-R_{m,(liquid)}]/ \\ [(n_{WS}A)^{-1/3}+(n_{WS}B)^{-1/3}] \qquad (5.25)$$

with:

$\Delta H^{f}\,A_{x_A}B_{x_B}(s)$:	enthalpy of formation of an alloy of composition $A_{x_A}B_{x_B}$;
$\Delta\overline{H}^{solv}{}_{A\text{ in }B}(l)$:	partial molar enthalpy of solution of component A in B at infinite dilution;
x_A and x_B:	mole fraction of component A and B, respectively ($x_A + x_B = 1$);
$V_{A,alloy}$:	atomic volume of component A within the alloy
f_B^A:	degree to which an atomic cell of metal A is in contact with dissimilar atomic cells of metal B on average, has been determined empirical for statistically ordered and ordered alloys [Boer, 1988];
P, Q:	empirical constants for specific combinations of metals, tabulated in [Boer, 1988];
$\Delta\Phi^*$:	difference of Miedema Electronegativities of the constituents;
Δn_{ws}:	difference of Electron densities at the Wigner-Seitz cell boundary of the constituents;
R_m:	hybridisation term that was introduced to account for an additional enthalpy contribution due to interaction of d- and p-orbitals in solid compounds of transition metals with non transition metals, treated as a group-specific constant within the Miedema model;
$R_{m,liquid}$:	for liquid mixtures a reduced hybridisation term has to be used: $R_{m,liquid} = 0.73R_m$;
ΔH^{trans} A, B:	enthalpies for the transformation of elements A and B into a hypothetical metallic state (for semi- or non-metallic elements).

For a detailed discussion of the model see [Boer, 1988].

A consistent set of Miedema parameters was developed for the elements of the chalcogen group (Group 16 of the periodic table of the elements: O, S, Se, Te, Po) from the results of quantum chemical calculations as well as empirical correlations with physical properties related to electronegativity and electron density [Neuhausen, 2003]. The values of these parameters are listed in Table 5.2.14. For details of the derivation of parameters we refer to the original literature [Neuhausen, 2003].

Table 5.2.14. Miedema parameters for the elements of the chalcogen group

Element	$n_{ws}^{1/3}$ [d.u.$^{1/3}$]	Φ* [V]	$V^{2/3}$ [cm^{2}mol$^{-2/3}$]
O	1.70	6.97	2.656
S	1.46	5.60	4.376
Se	1.40	5.17	5.172
Te	1.31	4.72	6.439
Po	1.15	4.44	7.043
Hybridisation term R for the chalcogen group: 2.45 V^2		Valence factor *a* for the chalcogen group: 0.04	

Using this parameter set, thermochemical properties such as enthalpies of formation of solid metal chalcogenides, partial molar enthalpies of solution of chalcogens in liquid and solid metals, partial molar enthalpies of evaporation of the chalcogens from liquid metal solution into the monoatomic gaseous state, partial molar enthalpies of adsorption of chalcogenides on metal surfaces at zero coverage and partial molar enthalpies of segregation of the chalcogens in trace amounts within solid metal matrices have been calculated. These properties are compared with available experimental data and discussed with an emphasis on the periodic behaviour of the elements. Systematic errors of the model for specific element combinations are discussed as well. As an example, Figure 5.2.3 shows a comparison of calculated formation enthalpies for metal sulphides (bars) with the corresponding literature data (squares) [Mills, 1974]. Shaded bars correspond to metal-sulphur combinations, where a systematic underestimation of stability is known for the Miedema model.

Figure 5.2.3. Calculated (bars) and tabulated (squares) enthalpies of formation for one mole of sulphides $M_{0.5}S_{0.5}$ vs. atomic number of the metal M

White bars indicate combinations of a transition element with sulphur, whereas combinations of sulphur with main group elements, where Brillouin zone effects lead to an underestimation of stability, are symbolised by shaded bars

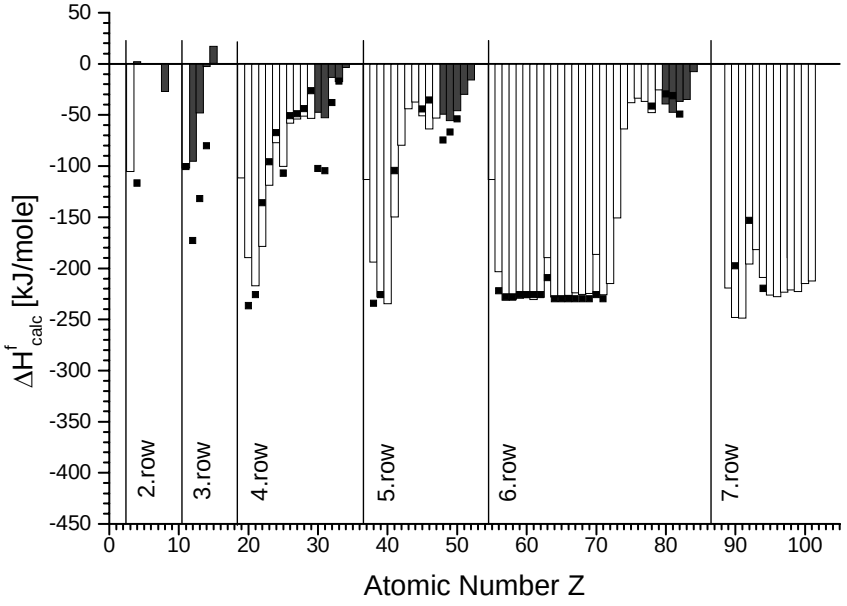

The model calculations show that a semi-quantitative description of the thermochemical properties of the chalcogens using the semi-empirical Miedema approach is possible. General trends in the formation enthalpies of metal chalcogenides throughout the periodic table are represented reasonably well by the results of calculations. It should be pointed out that the computed enthalpy values should not be considered as highly precise data. However, periodic trends and relative stabilities of series of compounds are reproduced well by the calculations Therefore, the calculated properties can serve as a basis for the prediction of the chemical interactions for metal-chalcogen combinations that have not been studied experimentally so far, i.e. especially for metal polonium combinations. Figure 5.2.4 shows a summary of calculated formation enthalpies of metal polonides of composition $M_{0.5}Po_{0.5}$ and the experimentally known qualitative facts about those metal polonium systems. In general, the agreement is satisfactory. For metal-polonium combinations were compound formation is observed, negative enthalpies of formation are calculated, whereas positive values are calculated for systems where no reaction is observed.

Enthalpy values for polonium-containing systems are compiled in Tables 5.2.15-5.2.17.

5.2.4 Analysis of thermochemical relations of iodine within a liquid LBE spallation target

For an assessment of the release properties of the halogens within a liquid LBE target, temperature dependant equilibrium constants for the formation reactions of halogen-containing species in the heterogeneous systems Pb/Bi/H/O/X (X = halogen) were calculated by Eichler, *et al*. [Eichler, 2003] using tabulated thermodynamic data [Barin, 1995]. Based on these evaluations no predominant pathway for the formation of gaseous iodine compounds can be found.

Because of the small concentrations and presumably low thermodynamic activity coefficients for non ideal behaviour an extensive release of iodine seems unlikely even at the given operating temperatures. Volatile iodine-containing species that could be present in the gaseous phase at very low concentrations are expected to react with basic oxides or hydroxides of nuclear reaction products, thus lowering the iodine gas phase concentration even more.

A basic absorber material (CaO, $Ca(OH)_2$) located in the gas plenum has promise to preclude the presence of small amounts of gaseous iodine species. In addition, this absorber would serve for the fixation of iodine produced within the gas phase by decay of Xe isotopes.

Figure 5.2.4. Experimental information and Miedema predictions of the stability of binary polonides throughout the periodic table of the elements

Each box corresponds to the binary system of the specified element with polonium. The atomic number of the element is given in brackets. The boxes are shaded as follows: white boxes = binary system not investigated; horizontally hatched boxes = no reaction is observed between the respective element and polonium; vertically hatched boxes = reaction is observed, but the product is not well characterised; cross hatched boxes = contradictory evidence from different literature; diagonally hatched boxes = reaction is observed, reaction product characterised by x-ray diffraction or at least melting or decomposition temperature has been determined. Values for the enthalpies of formation of solid compounds of composition $M_{0.5}Po_{0.5}$ calculated using the Miedema model are given for each combination. The box for La(57) can be considered representative for the complete lanthanide series.

Table 5.2.15. Calculated enthalpies of formation (ΔH^{f}_{calc}) of solid binary polonides obtained using Miedema parameters derived in [Neuhausen, 2003] (Table 5.2.14)

All other Miedema parameters have been taken from [Boer, 1988]. For comparison, the few available literature data and values calculated by other methods within [Neuhausen, 2003] have been included (ΔH^{f}_{Lit})

Partner element	Composition $M_{1-x}Po_x$	ΔH^{f}_{calc} [kJmol^{-1}]	ΔH^{f}_{Lit} [kJmol^{-1}]
Ac	0.3333	-114.3	
	0.5000	-135.8	
	0.6000	-125.0	
	0.6667	-109.6	
Ag	0.3333	1.2	
	0.5000	1.2	
	0.6000	1.1	
	0.6667	0.9	
Al	0.3333	12.9	
	0.5000	13.2	
	0.6000	11.3	
	0.6667	9.6	
Am	0.3333	-99.8	
	0.5000	-113.1	
	0.6000	-101.6	
	0.6667	-88.0	
As	0.3333	18.5	
	0.5000	20.2	
	0.6000	17.8	
	0.6667	15.2	
Au	0.3333	13.5	
	0.5000	14.5	
	0.6000	12.7	
	0.6667	10.8	
B	0.3333	82.2	
	0.5000	70.2	
	0.6000	57.0	
	0.6667	47.4	
Ba	0.3333	-115.0	
	0.5000	-149.3	-153[a] -161.5[b] -167.8[g] -137.7[h] -137.6[k]
	0.6000	-143.9	
	0.6667	-129.1	
Be	0.3333	51.0	
	0.5000	45.7	-28.6[b]
	0.6000	37.3	
	0.6667	31.1	
Bi	0.3333	-2.3	
	0.5000	-2.8	
	0.6000	-2.6	
	0.6667	-2.3	

Table 5.2.15. Calculated enthalpies of formation (ΔH^{f}_{calc}) of solid binary polonides obtained using Miedema parameters derived in [Neuhausen, 2003] (Table 5.2.14) (*cont.*)

All other Miedema parameters have been taken from [Boer, 1988]. For comparison, the few available literature data and values calculated by other methods within [Neuhausen, 2003] have been included (ΔH^{f}_{Lit})

Partner element	Composition $M_{1-x}Po_x$	ΔH^{f}_{calc} [kJmol^{-1}]	ΔH^{f}_{Lit} [kJmol^{-1}]
Bk	0.3333	-100.1	
	0.5000	-112.1	
	0.6000	-100.0	
	0.6667	-86.3	
C	0.3333	127.5	
	0.5000	96.3	
	0.6000	77.1	
	0.6667	64.2	
Ca	0.3333	-103.3	
	0.5000	-123.3	-128[a] -140.4[b] -132.1[c] -135.9[g] -117.3[h] -121.3[k]
	0.6000	-112.9	
	0.6667	-98.7	
Cd	0.3333	-2.0	
	0.5000	-2.2	-1.8[b] -29.2[c]
	0.6000	-1.9	
	0.6667	-1.7	
Ce	0.3333	-108.7	
	0.5000	-129.6	
	0.6000	-119.6	
	0.6667	-105.0	
Cf	0.3333	-96.9 (Cf(II)) -99.9(Cf(III))	
	0.5000	-119.4 (Cf(II)) -111.2 (Cf(III))	
	0.6000	-111.6 (Cf(II)) -98.9 (Cf(III))	
	0.6667	-98.6 (Cf(II)) -85.3 (Cf(III))	
Cm	0.3333	-99.0	
	0.5000	-113.0	
	0.6000	-101.8	
	0.6667	-88.3	
Co	0.3333	15.1	
	0.5000	14.3	
	0.6000	11.9	
	0.6667	10.0	
Cr	0.3333	20.6	
	0.5000	19.8	
	0.6000	16.5	
	0.6667	13.8	

Table 5.2.15. Calculated enthalpies of formation (ΔH^{f}_{calc}) of solid binary polonides obtained using Miedema parameters derived in [Neuhausen, 2003] (Table 5.2.14) (*cont.*)

All other Miedema parameters have been taken from [Boer, 1988]. For comparison, the few available literature data and values calculated by other methods within [Neuhausen, 2003] have been included (ΔH^{f}_{Lit})

Partner element	Composition $M_{1-x}Po_x$	ΔH^{f}_{calc} [kJmol^{-1}]	ΔH^{f}_{Lit} [kJmol^{-1}]
Cs	0.3333	-55.8	-114[a]
	0.5000	-79.1	
	0.6000	-80.9	
	0.6667	-74.5	
Cu	0.3333	6.5	
	0.5000	6.2	
	0.6000	5.1	
	0.6667	4.3	
Dy	0.3333	-104.9	
	0.5000	-121.1	-115.2[b] -154.0[g]
	0.6000	-109.8	
	0.6667	-95.5	
Er	0.3333	-103.6	
	0.5000	-118.7	
	0.6000	-107.2	
	0.6667	-93.1	
Es	0.3333	-116.0	
	0.5000	-143.9	
	0.6000	-134.9	
	0.6667	-119.3	
Eu	0.3333	-103.5 (Eu(II)) -42.3 (Eu(III))	
	0.5000	-126.6 (Eu(II)) -76.3 (Eu(III))	-147.8[b] -152.7[g] -111[h]
	0.6000	-117.5 (Eu(II)) -75.1 (Eu(III))	
	0.6667	-103.4 (Eu(II)) -67.1 (Eu(III))	
Fe	0.3333	28.6	
	0.5000	27.4	
	0.6000	22.9	
	0.6667	19.2	
Fm	0.3333	-111.1	
	0.5000	-132.4	
	0.6000	-121.3	
	0.6667	-106.1	
Ga	0.3333	3.4	
	0.5000	3.6	
	0.6000	3.1	
	0.6667	2.7	
Gd	0.3333	-106.3	
	0.5000	-124.1	
	0.6000	-113.2	
	0.6667	-98.8	

Table 5.2.15. Calculated enthalpies of formation (ΔH^{f}_{calc}) of solid binary polonides obtained using Miedema parameters derived in [Neuhausen, 2003] (Table 5.2.14) (*cont.*)

All other Miedema parameters have been taken from [Boer, 1988]. For comparison, the few available literature data and values calculated by other methods within [Neuhausen, 2003] have been included (ΔH^{f}_{Lit})

Partner element	Composition $M_{1-x}Po_x$	ΔH^{f}_{calc} [kJmol^{-1}]	ΔH^{f}_{Lit} [kJmol^{-1}]
Ge	0.3333	28.4	
	0.5000	24.6	
	0.6000	20.4	
	0.6667	17.1	
H	0.3333	74.5	
	0.5000	56.0	
	0.6000	44.8	
	0.6667	37.3	
Hf	0.3333	-77.9	
	0.5000	-84.4	-2.8[b] -3.4[c]
	0.6000	-74.3	
	0.6667	-63.7	
Hg	0.3333	0.5	
	0.5000	0.6	-10.5[b] 3.7[c]
	0.6000	0.5	
	0.6667	0.4	
Ho	0.3333	-103.9	
	0.5000	-119.6	-116.8[b] -141.4[g] -132[h]
	0.6000	-108.2	
	0.6667	-94.1	
In	0.3333	-7.8	
	0.5000	-8.8	
	0.6000	-7.9	
	0.6667	-6.9	
Ir	0.3333	21.8	
	0.5000	22.3	
	0.6000	19.1	
	0.6667	16.2	
K	0.3333	-53.4	-123[a]
	0.5000	-70.4	
	0.6000	-67.5	
	0.6667	-60.1	
La	0.3333	-109.8	
	0.5000	-132.2	
	0.6000	-122.7	
	0.6667	-108.1	
Li	0.3333	-52.8	
	0.5000	-50.9	
	0.6000	-42.5	
	0.6667	-35.8	

Table 5.2.15. Calculated enthalpies of formation (ΔH^{f}_{calc}) of solid binary polonides obtained using Miedema parameters derived in [Neuhausen, 2003] (Table 5.2.14) (*cont.*)

All other Miedema parameters have been taken from [Boer, 1988]. For comparison, the few available literature data and values calculated by other methods within [Neuhausen, 2003] have been included (ΔH^{f}_{Lit})

Partner element	Composition $M_{1-x}Po_x$	ΔH^{f}_{calc} [kJmol^{-1}]	ΔH^{f}_{Lit} [kJmol^{-1}]
Lu	0.3333	-103.0	
	0.5000	-116.8	-72.6[b] -8.8[c] -13.6[g]
	0.6000	-105.0	
	0.6667	-90.9	
Mg	0.3333	-25.9	
	0.5000	-27.5	-27[a] -56.9[c]
	0.6000	-23.9	
	0.6667	-20.4	
Mn	0.3333	-13.9	
	0.5000	-13.3	
	0.6000	-11.1	
	0.6667	-9.3	
Mo	0.3333	37.5	
	0.5000	38.3	
	0.6000	32.8	
	0.6667	27.7	
N	0.3333	130.4	
	0.5000	87.2	
	0.6000	68.9	
	0.6667	57.5	
Na	0.3333	-47.7	-116[a]
	0.5000	-54.2	
	0.6000	-48.0	
	0.6667	-41.3	
Nb	0.3333	-11.7	
	0.5000	-12.1	40.9[c]
	0.6000	-10.5	
	0.6667	-8.9	
Nd	0.3333	-107.5	
	0.5000	-126.5	
	0.6000	-116.0	
	0.6667	-101.5	
Ni	0.3333	10.7	
	0.5000	10.2	-23.6[b] 6.3[c] -23.4[h] -19.2[i]
	0.6000	8.5	
	0.6667	7.1	
Np	0.3333	-59.3	
	0.5000	-62.2	
	0.6000	-53.9	
	0.6667	-45.9	
O	0.3333	-79.9	-84.2 (8.4)d -84.4e -83.7f
	0.5000	-72.2	
	0.6000	-58.9	
	0.6667	-49.0	

Table 5.2.15. Calculated enthalpies of formation (ΔH^{f}_{calc}) of solid binary polonides obtained using Miedema parameters derived in [Neuhausen, 2003] (Table 5.2.14) (*cont.*)

All other Miedema parameters have been taken from [Boer, 1988]. For comparison, the few available literature data and values calculated by other methods within [Neuhausen, 2003] have been included (ΔH^{f}_{Lit})

Partner element	Composition $M_{1-x}Po_x$	ΔH^{f}_{calc} [kJmol^{-1}]	ΔH^{f}_{Lit} [kJmol^{-1}]
Os	0.3333	40.6	
	0.5000	41.4	
	0.6000	35.3	
	0.6667	29.8	
P	0.3333	41.8	
	0.5000	39.7	
	0.6000	33.5	
	0.6667	28.2	
Pa	0.3333	-118.9	
	0.5000	-131.3	
	0.6000	-116.6	
	0.6667	-100.4	
Pb	0.3333	-3.1	
	0.5000	-3.7	-29.4[b] -18.2[c] -33.9[h] -28.3[k]
	0.6000	-3.5	
	0.6667	-3.0	
Pd	0.3333	-29.6	
	0.5000	-30.7	-29.4[c]
	0.6000	-26.3	
	0.6667	-22.3	
Pm	0.3333	-107.4	
	0.5000	-125.9	
	0.6000	-115.1	
	0.6667	-100.6	
Pr	0.3333	-107.6	
	0.5000	-127.0	
	0.6000	-116.6	
	0.6667	-102.1	
Pt	0.3333	-6.0	
	0.5000	-6.3	
	0.6000	-5.4	
	0.6667	-4.6	-23.3[b] -27.4[c] -13.8[h] -10.5[i]
Pu	0.3333	-84.9	
	0.5000	-89.2	
	0.6000	-77.4	
	0.6667	-65.9	
Rb	0.3333	-55.0	-112a
	0.5000	-75.4	
	0.6000	-74.6	
	0.6667	-67.4	
Re	0.3333	52.6	
	0.5000	53.9	
	0.6000	46.2	
	0.6667	39.1	

Table 5.2.15. Calculated enthalpies of formation (ΔH^{f}_{calc}) of solid binary polonides obtained using Miedema parameters derived in [Neuhausen, 2003] (Table 5.2.14) (*cont.*)

All other Miedema parameters have been taken from [Boer, 1988]. For comparison, the few available literature data and values calculated by other methods within [Neuhausen, 2003] have been included (ΔH^{f}_{Lit})

Partner element	Composition $M_{1-x}Po_x$	ΔH^{f}_{calc} [kJmol^{-1}]	ΔH^{f}_{Lit} [kJmol^{-1}]
Rh	0.3333	4.1	
	0.5000	4.1	
	0.6000	3.5	
	0.6667	3.0	
Ru	0.3333	31.7	
	0.5000	32.0	
	0.6000	27.2	
	0.6667	23.0	
S	0.3333	-11.6	
	0.5000	-12.2	
	0.6000	-10.5	
	0.6667	-8.9	
Sb	0.3333	3.1	
	0.5000	3.7	
	0.6000	3.4	
	0.6667	3.0	
Sc	0.3333	-97.1	
	0.5000	-105.5	-81.1[b] -92.5[c] -76.7[g] -124[h]
	0.6000	-92.8	
	0.6667	-79.6	
Se	0.3333	1.5	
	0.5000	1.6	
	0.6000	1.5	
	0.6667	1.3	
Si	0.3333	51.5	
	0.5000	45.8	
	0.6000	38.1	
	0.6667	32.0	
Sm	0.3333	-106.4	
	0.5000	-124.4	
	0.6000	-113.6	
	0.6667	-99.2	
Sn	0.3333	-0.2	
	0.5000	-0.3	
	0.6000	-0.2	
	0.6667	-0.2	
Sr	0.3333	-106.6	
	0.5000	-135.1	-134a -155.6b -141.6c -156.2g
	0.6000	-128.2	
	0.6667	-114.0	
Ta	0.3333	-14.7	
	0.5000	-15.3	76.4c
	0.6000	-13.2	
	0.6667	-11.2	

Table 5.2.15. Calculated enthalpies of formation (ΔH^{f}_{calc}) of solid binary polonides obtained using Miedema parameters derived in [Neuhausen, 2003] (Table 5.2.14) (*cont.*)

All other Miedema parameters have been taken from [Boer, 1988]. For comparison, the few available literature data and values calculated by other methods within [Neuhausen, 2003] have been included (ΔH^{f}_{Lit})

Partner element	Composition $M_{1-x}Po_x$	ΔH^{f}_{calc} [kJmol^{-1}]	ΔH^{f}_{Lit} [kJmol^{-1}]
Tb	0.3333	-105.1	
	0.5000	-121.9	-112.7[b] -108.0[g]
	0.6000	-110.7	
	0.6667	-96.5	
Tc	0.3333	29.7	
	0.5000	30.3	
	0.6000	25.9	
	0.6667	21.9	
Te	0.3333	4.6	
	0.5000	5.4	
	0.6000	5.0	
	0.6667	4.3	
Th	0.3333	-108.7	
	0.5000	-128.3	
	0.6000	-118.2	
	0.6667	-103.7	
Ti	0.3333	-51.4	
	0.5000	-52.7	-29.6[b] -29.2[c] -47.5[g] -45.5[h] -24.8[i]
	0.6000	-45.2	
	0.6667	-38.3	
Tl	0.3333	-7.6	
	0.5000	-8.8	
	0.6000	-8.0	
	0.6667	-7.0	
Tm	0.3333	-103.4	
	0.5000	-117.9	-120.4b -144.8g
	0.6000	-106.2	
	0.6667	-92.1	
U	0.3333	-68.1	
	0.5000	-72.6	
	0.6000	-63.4	
	0.6667	-54.2	
V	0.3333	-7.2	
	0.5000	-7.1	43.1c
	0.6000	-6.0	
	0.6667	-5.0	
W	0.3333	51.2	
	0.5000	52.9	
	0.6000	45.4	
	0.6667	38.5	
Y	0.3333	-106.3	
	0.5000	-124.1	-100.4b -102.3c -38.8g
	0.6000	-113.2	
	0.6667	-98.8	

Table 5.2.15. Calculated enthalpies of formation (ΔH^{f}_{calc}) of solid binary polonides obtained using Miedema parameters derived in [Neuhausen, 2003] (Table 5.2.14) (*cont.*)

All other Miedema parameters have been taken from [Boer, 1988]. For comparison, the few available literature data and values calculated by other methods within [Neuhausen, 2003] have been included (ΔH^{f}_{Lit})

Partner element	Composition $M_{1-x}Po_x$	ΔH^{f}_{calc} [kJmol^{-1}]	ΔH^{f}_{Lit} [kJmol^{-1}]
Yb	0.3333	-101.6 (Yb(II)) -75.9 (Yb(III))	
	0.5000	-119.8 (Yb(II)) -97.0 (Yb(III))	-114.0[b] -122.2[g] -125[h]
	0.6000	-108.9 (Yb(II)) -89.3 (Yb(III))	
Yb	0.6667	-94.9 (Yb(II)) -78.0 (Yb(III))	
Zn	0.3333	4.0	
	0.5000	3.9	-24.1[c]
	0.6000	3.3	
	0.6667	2.8	
Zr	0.3333	-94.1	
	0.5000	-102.5	-27.6[b] -38.1[c]
	0.6000	-90.5	
	0.6667	-77.7	

[a] [Krestov, 1962].
[b] LMTO calculations [Neuhausen, 2003].
[c] PP-PW calculations [Neuhausen, 2003].
[d] [Brewer, 1953].
[e] [Latimer, 1952].
[f] [Zhdanov, 1985].
[g] Calculated from Kapustinskii lattice energies, ionisation energies and sublimation enthalpies [Neuhausen, 2003].
[h] Estimated from linear correlations with lnA in homologous series MQ (Q = S, Se, Te) [Neuhausen, 2003].
[i] Estimated from linear correlations with covalent radius of the chalcogen in homologous series MQ (Q = S, Se, Te) [Neuhausen, 2003].
[k] Estimated from linear correlations with ionic radius of the chalcogen in homologous series MQ (Q = S, Se, Te) [Neuhausen, 2003].

Table 5.2.16. Calculated values for the partial molar enthalpy of solution of liquid polonium in liquid elements B at infinite dilution and calculated partial molar enthalpies of evaporation of polonium into the monoatomic state from liquid metal solutions [Neuhausen, 2003]

Symbol of element B	Atomic number Z	$\Delta\overline{H}^{solv}_{Poin\ B(l)}$ (calc.) [kJmol^{-1}]	$\Delta\overline{H}^{v}_{Poin\ B(l)}$ (calc.) [kJmol^{-1}]
Ac	89	-322.4	511.3
Ag	47	15.0	173.9
Al	13	46.5	142.4
Am	95	-279.3	468.2
As	33	63.0	125.9
Au	79	69.3	119.6
B	5	268.1	-79.2
Ba	56	-335.5	524.4
Be	4	218.1	-29.2
Bi	83	-7.3	196.2
Bk	97	-282.8	471.7
C	6	36.5	152.4
Ca	20	-309.6	498.5
Cd	48	-7.0	195.9
Ce	58	-301.8	490.7
CfII	98	-285.8	474.7
CfIII	98	-283.3	472.2
Cm	96	-275.6	464.5
Co	27	136.3	52.6
Cr	24	158.4	30.5
Cs	55	-174.3	363.2
Cu	29	47.8	141.1
Dy	66	-293.8	482.7
Er	68	-290.6	479.5
Es	99	-342.5	531.4
EuII	63	-308.3	497.2
EuIII	63	-296.7	485.6
Fe	26	188.4	0.5
Fm	100	-331.1	520.0
Ga	31	11.7	177.2
Gd	64	-296.7	485.6
Ge	32	41.7	147.2
Hf	72	-190.1	379.0
Hg	80	1.7	187.2
Ho	67	-291.0	479.9
In	49	-25.8	214.7
Ir	77	155.7	33.2
K	19	-167.1	356.0
La	57	-304.1	493.0
Li	3	-192.1	381.0
Lu	71	-290.0	478.9
Mg	12	-89.0	277.9
Mn	25	23.4	165.5
Mo	42	214.1	-25.2

Table 5.2.16. Calculated values for the partial molar enthalpy of solution of liquid polonium in liquid elements B at infinite dilution and calculated partial molar enthalpies of evaporation of polonium into the monoatomic state from liquid metal solutions [Neuhausen, 2003] (*cont.*)

Symbol of element B	Atomic number Z	$\Delta\overline{H}^{solv}_{\text{Poin B(l)}}$ (calc.) [kJmol^{-1}]	$\Delta\overline{H}^{v}_{\text{Poin B(l)}}$ (calc.) [kJmol^{-1}]
Na	11	-155.2	344.1
Nb	41	37.8	151.1
Nd	60	-299.4	488.3
Ni	28	119.1	69.8
Np	93	-131.4	320.3
Os	76	224.9	-36.0
P	15	109.5	79.4
Pa	91	-327.7	516.6
Pb	82	-10.2	199.1
Pd	46	-30.3	219.2
Pm	61	-299.5	488.4
Po	84	0	188.9
Pr	59	-299.4	488.3
Pt	78	55.3	133.6
Pu	94	-221.3	410.2
Rb	37	-171.7	360.6
Re	75	267.9	-79.0
Rh	45	91.6	97.3
Ru	44	193.3	-4.4
S	16	-41.0	229.9
Sb	51	10.2	178.7
Sc	21	-278.6	467.5
Se	34	5.1	183.8
Si	14	105.6	83.3
Sm	62	-296.7	485.6
Sn	50	-0.7	189.6
Sr	38	-315.6	504.5
Ta	73	26.8	162.1
Tb	65	-293.8	482.7
Tc	43	185.0	3.9
Te	52	14.9	174.0
Th	90	-302.7	491.6
Ti	22	-106.4	295.3
Tl	81	-24.8	213.7
Tm	69	-290.6	479.5
U	92	-159.1	348.0
V	23	51.2	137.7
W	74	262.4	-73.5
Y	39	-296.7	485.6
YbII	70	-305.5	494.4
YbIII	70	-290.6	479.5
Zn	30	14.7	174.2
Zr	40	-244.4	433.3

Table 5.2.17. Calculated values for the partial molar enthalpy of solution of polonium in solid elements B at infinite dilution, mechanism of polonium adsorption on/in solid surfaces of element B, see [Neuhausen, 2003], partial molar enthalpies of adsorption of polonium in/on solid surfaces of B at zero coverage, partial molar net enthalpies of adsorption of polonium in/on solid surfaces of B at zero coverage and partial molar enthalpies of segregation of polonium in a solid matrix of B

Element B	Atomic number Z	$\Delta\overline{H}^{solv}_{\text{Po in B (s)}}$ (calc.) [kJmol^{-1}]	Adsorption mechanism	$\Delta\overline{H}^{ads}_{\text{Po in/on B}}$ (calc.) [kJmol^{-1}]	$\Delta\overline{H}^{ads,net}_{\text{Po in/on B}}$ (calc.) [kJmol^{-1}]	$\Delta\overline{H}^{seg}$ Po (calc.) [kJmol^{-1}]
Ac	89	-369.8	In	-540.7	-351.8	18.1
Ag	47	4.2	In	-212.8	-23.9	-28.1
Al	13	46.5	In (on)	-167.8 (-227.8)	21.1 (-38.9)	-25.4 (-85.4)
Am	95	-330.1	In	-509.6	-320.7	9.3
As	33	63.0	On	-221.3	-32.4	-95.4
Au	79	47.0	In (on)	-175.8 (-254.6)	13.1 (-65.7)	-33.9 (-112.7)
B	5	268.1	On	-303.2	-114.3	-382.3
Ba	56	-361.3	In	-524.2	-335.3	26
Be	4	218.1	On	-243.9	-55	-273
Bi	83	-7.3	In	-203.6	-14.7	-7.3
Bk	97	-333.6	In	-511.4	-322.5	11.1
C	6	36.5	In	-375.2	-186.3	-222.8
Ca	20	-331.5	In	-501.6	-312.7	18.8
Cd	48	-7.0	In	-206.7	-17.8	-10.8
Ce	58	-351.3	In	-520.4	-331.5	19.8
CfII	98	-308.4	In	-503.6	-314.7	19.2
CfIII	98	-333.9	In	-486.5	-297.6	10.8
Cm	96	-326.5	In	-508.8	-319.9	6.6
Co	27	58.6	On (in)	-318.5 (-187.4)	-129.6 (1.5)	-188.2 (-57.0)
Cr	24	79.6	On	-337.5	-148.6	-228.2
Cs	55	-174.3	In	-347.8	-158.9	15.4
Cu	29	25.5	In	-204.7	-15.8	-41.3
Dy	66	-343.8	In	-524.5	-335.6	8.2
Er	68	-340.8	In	-524.2	-335.3	5.5
Es	99	-368.2	In	-533.6	-344.7	23.4
EuII	63	-329.8	In	-514.0	-325.1	21.4
EuIII	63	-346.5	In	-502.2	-313.3	16.5
Fe	26	109.8	On	-286.5	-97.6	-207.4
Fm	100	-357.3	In	-534.2	-345.3	12
Ga	31	11.7	In	-184.6	4.3	-7.4
Gd	64	-346.5	In	-524.7	-335.8	10.7
Ge	32	41.7	In (on)	-179.0 (-252.9)	9.9 (-64.0)	-31.8 (-105.7)
Hf	72	-266.3	In	-477.0	-288.1	-21.8
Hg	80	1.7	In	-191.7	-2.8	-4.4
Ho	67	-341.0	In	-523.2	-334.3	6.7
In	49	-25.8	In	-219.5	-30.6	-4.8
Ir	77	78.0	On	-353.8	-164.9	-242.9
K	19	-167.1	In	-342.3	-153.4	13.7
La	57	-353.4	In	-523.5	-334.6	18.8
Li	3	-192.1	In	-371.0	-182.1	10
Lu	71	-340.4	In	-526.8	-337.9	2.6
Mg	12	-89.0	In	-286.5	-97.6	-8.5
Mn	25	-53.8	In	-279.7	-90.8	-37
Mo	42	134.6	On	-327.4	-138.5	-273.1
Na	11	-155.2	In	-333.7	-144.8	10.5
Nb	41	-41.2	In (on)	-286.4 (-407.7)	-97.4 (-218.8)	-56.2 (-177.6)

Table 5.2.17. Calculated values for the partial molar enthalpy of solution of polonium in solid elements B at infinite dilution, mechanism of polonium adsorption on/in solid surfaces of element B, see [Neuhausen, 2003], partial molar enthalpies of adsorption of polonium in/on solid surfaces of B at zero coverage, partial molar net enthalpies of adsorption of polonium in/on solid surfaces of B at zero coverage and partial molar enthalpies of segregation of polonium in a solid matrix of B (*cont.*)

Element B	Atomic number Z	$\Delta\overline{H}^{solv}_{\text{Po in B (s)}}$ (calc.) [kJmol^{-1}]	Adsorption mechanism	$\Delta\overline{H}^{ads}_{\text{Po in/on B}}$ (calc.) [kJmol^{-1}]	$\Delta\overline{H}^{ads,net}_{\text{Po in/on B}}$ (calc.) [kJmol^{-1}]	$\Delta\overline{H}^{seg}$ Po (calc.) [kJmol^{-1}]
Nd	60	-349.0	In	-522.1	-333.2	15.8
Ni	28	41.7	In (on)	-201.6 (-325.6)	-12.7 (-136.7)	-54.4 (-178.4)
Np	93	-207.8	In	-395.3	-206.4	1.4
Os	76	146.4	On	-361.3	-172.4	-318.8
P	15	109.5	On	-191.3	-2.4	-111.9
Pa	91	-401.2	In	-583.4	-394.5	6.6
Pb	82	-10.2	In	-207.3	-18.4	-8.2
Pd	46	-105.5	In	-327.1	-138.2	-32.6
Pm	61	-349.3	In	-522.9	-334	15.3
Po	84	0	In	-196.8	-7.9	-7.9
Pr	59	-349.0	In	-520.7	-331.8	17.2
Pt	78	-21.2	In	-255.0	-66.1	-44.9
Pu	94	-296.7	In	-474.7	-285.8	10.9
Rb	37	-171.7	In	-345.9	-157	14.7
Re	75	188.8	On	-341.9	-153	-341.8
Rh	45	14.7	In	-231.1	-42.2	-56.9
Ru	44	115.2	On	-329.6	-140.7	-255.9
S	16	-41.0	In	-234.9	-46	-4.9
Sb	51	10.2	In	-194.2	-5.3	-15.5
Sc	21	-329.5	In	-518.4	-329.5	0
Se	34	5.1	In	-194.1	-5.2	-10.3
Si	14	105.6	On	-260.7	-71.8	-177.4
Sm	62	-346.5	In	-521.0	-332.1	14.4
Sn	50	-0.7	In	-197.9	-9	-8.3
Sr	38	-336.6	In	-503.3	-314.4	22.2
Ta	73	-52.0	In	-307.8	-118.9	-66.9
Tb	65	-343.8	In	-523.4	-334.5	9.3
Tc	43	106.9	on	-314.1	-125.2	-232.1
Te	52	14.9	In	-187.2	1.7	-13.2
Th	90	-353.5	In	-537.5	-348.6	4.9
Ti	22	-183.7	In	-397.8	-208.9	-25.2
Tl	81	-24.8	In	-220.6	-31.7	-6.8
Tm	69	-340.8	In	-524.8	-335.9	4.9
U	92	-235.3	In	-428.0	-239.1	-3.7
V	23	-27.2	In	-269.7	-80.8	-53.6
W	74	182.7	On	-354.3	-165.4	-348
Y	39	-346.5	In	-527.9	-339	7.6
YbII	70	-327.5	In	-501.3	-312.4	15.1
YbIII	70	-340.8	In	-510.2	-321.3	19.5
Zn	30	14.7	In	-192.6	-3.7	-18.4
Zr	40	-320.1	In	-517.2	-328.3	-8.2

5.3 Investigations on irradiated LBE

5.3.1 Release of volatile radionuclides

In a critical system the production of radionuclides will be limited to isotopes near that of the target material. These elements will include polonium and mercury. However, in a spallation target using liquid LBE as a target material, isotopes of practically all chemical elements, ranging from hydrogen up to polonium, will be produced by different nuclear reactions. Among these nuclear reaction products there will be several elements which have to be considered more or less volatile at the operation conditions of the target. Table 5.3.1. lists the total inventory of the most important volatile elements which would be expected for a 200 d irradiation of the MEGAPIE target planned to be irradiated at PSI with 1.4 mA of 575 MeV protons based on the results of neutronics calculations using FLUKA and ORIHET3 [Zanini, 2005]. Among these elements, polonium and mercury have to be considered the most relevant from the radiation protection point of view. While polonium as an α-emitter is problematic mainly because of its high radiotoxicity, the importance of mercury arises from the fact that it is the element produced at largest quantities and, at the same time, it is the element with the by far highest volatility.

Table 5.3.1. Production of volatile elements within the MEGAPIE target calculated using the FLUKA/ORIHET3 codes for an irradiation with 1.4 mA of 575 MeV protons for 200 days

Element	Mass produced m [g]	Mole fraction in target x	Total activity [Bq]	n produced [mol]
Po	2.9	$3.3*10^{-6}$	$1.1*10^{15}$	$1.4*10^{-2}$
Bi	79.5	0.553	$4.3*10^{15}$	$3.8*10^{-1}$
Pb	100	0.447	$5.7*10^{15}$	$4.9*10^{-1}$
Tl	7.5	$8.9*10^{-6}$	$4.5*10^{15}$	$3.7*10^{-2}$
Hg	18.9	$2.3*10^{-5}$	$1.5*10^{15}$	$9.5*10^{-2}$
Xe	$2.0*10^{-2}$	$3.8*10^{-8}$	$2.1*10^{12}$	$1.6*10^{-4}$
I	$8.9*10^{-3}$	$1.7*10^{-8}$	$5.8*10^{12}$	$7.0*10^{-5}$
Cs	$1.4*10^{-3}$	$2.5*10^{-9}$	$2.8*10^{12}$	$1.0*10^{-5}$
Cd	$1.9*10^{-1}$	$4.1*10^{-7}$	$7.2*10^{12}$	$1.7*10^{-3}$
Kr	$1.6*10^{-1}$	$4.7*10^{-7}$	$1.9*10^{13}$	$2.0*10^{-3}$
Rb	$7.5*10^{-2}$	$2.1*10^{-7}$	$3.7*10^{13}$	$8.8*10^{-4}$
Br	$3.4*10^{-2}$	$1.0*10^{-7}$	$2.6*10^{13}$	$4.2*10^{-4}$

For radioprotection issues it is important to assess the behaviour of these elements during normal and off-normal operation conditions. In the following, we will discuss evaporation for the case of the MEGAPIE target as an example.

Under normal operating conditions a certain fraction of each volatile element will be evaporated to the cover gas of the target. In the following, we assume that the maximum vapour phase concentration that can be reached by release from LBE to the gas phase corresponds to the equilibrium vapour pressure, which can be calculated according to:

$$p_A = \gamma_A * x_A * p_A^\circ \tag{5.26}$$

where p_A is the equilibrium vapour pressure of the component A over the mixture, x_A is the mole fraction of the dissolved component A, γ_A is the thermodynamic activity coefficient of the dissolved component A and p_A is the vapour pressure of the pure component A.

Assuming ideal behaviour of the gaseous phase, the amount n (in moles) of volatiles in the gas phase of the expansion tank can then be calculated by:

$$n_A = p_A V/(RT) \tag{5.27}$$

where n_A is the amount of volatile A in the gas phase (moles), p is the vapour pressure of the volatile A (Pa), V is the cover gas volume (m^3), R is the universal gas constant (8.314 $Jmol^{-1}K^{-1}$) and T is the temperature in K.

The behaviour of volatiles in off-normal conditions will depend on the actual accident scenario and may include interaction with air, water and cooling liquids. A simple method for the estimation of maximum release rates will be given in Section 5.3.3.

5.3.1.1 Polonium vaporisation

For polonium, different vapour species and vaporisation reactions have been discussed in literature. The most prominent of these species are PbPo and H_2Po. BiPo or Po_2 molecules have not received much consideration. Given the actual state of research on polonium release from LBE we cannot be sure which of the above mentioned species would be the prominent form of polonium to be released from the liquid LBE. However, for an assessment of the source terms for polonium release in normal operation as well as in accident scenarios, this question does not have to be answered as long as a quantification of polonium in the gas phase is possible as a function of operating conditions such as temperature and composition. For this purpose, we can rely on experimental data in comparison with values obtained by extrapolation of thermodynamical functions [Eichler, 2002] and semi-empirical calculations [Neuhausen, 2003]. As most of the available experimental data are based on measurements performed at higher temperatures, we have to rely on extrapolations to lower temperature to assess the behaviour at the typical operating condition-approximately 450 to 650 K.

In the following we will discuss data on polonium release from liquid metals obtained by different authors. In general, experimental results on polonium release from liquid metals such as Bi or LBE show that much lower vapour pressures or evaporation rates are found for polonium dissolved in Bi [Joy, 1963] or LBE [Tupper, 1991], [Buongiorno, 2003], [Neuhausen, 2004] than would be expected from literature values for the vapour pressure of pure polonium [Brooks, 1955], [Abakumov, 1974]. This indicates that the thermodynamic activity coefficient for polonium in liquid Bi or LBE solution is <1. Figure 5.3.1 shows a comparison of values for the effective vapour pressure of polonium at a mole fraction of $3.3*10^{-6}$ in LBE solution (MEGAPIE target after an irradiation of 200 d with 1.4 mA of 572 MeV protons) obtained from different studies as well as from experiments performed at PSI.

Joy studied the vapour-liquid equilibrium of dilute solutions of polonium in liquid bismuth ($x \approx 10^{-6}$ to 10^{-10}) under vacuum [Joy, 1963]. From his experimental data he derived the following relation for the thermodynamic activity coefficient of dilute polonium in bismuth for the temperature range between 723 and 1123 K based on the vapour pressure relation obtained for the temperature range between 711 and 1018 K from [Brooks, 1955]:

$$\log \gamma_{Po} = -2728.3/T[K] + 1.1176 \tag{5.28}$$

$$\log p_{Po}[Torr] = -5377.8/T[K] + 7.2345 \tag{5.29}$$

Figure 5.3.1. Effective vapour pressure of polonium over a diluted solution ($x = 3.3*10^{-6}$) of polonium in bismuth [Joy, 1963], [Brooks, 1955]) or LBE [Buongiorno, 2003], [Neuhausen, 2004], together with theoretically derived data

Values corresponding to the temperature regime experimentally investigated are depicted as full symbols, while extrapolated data are shown as open symbols

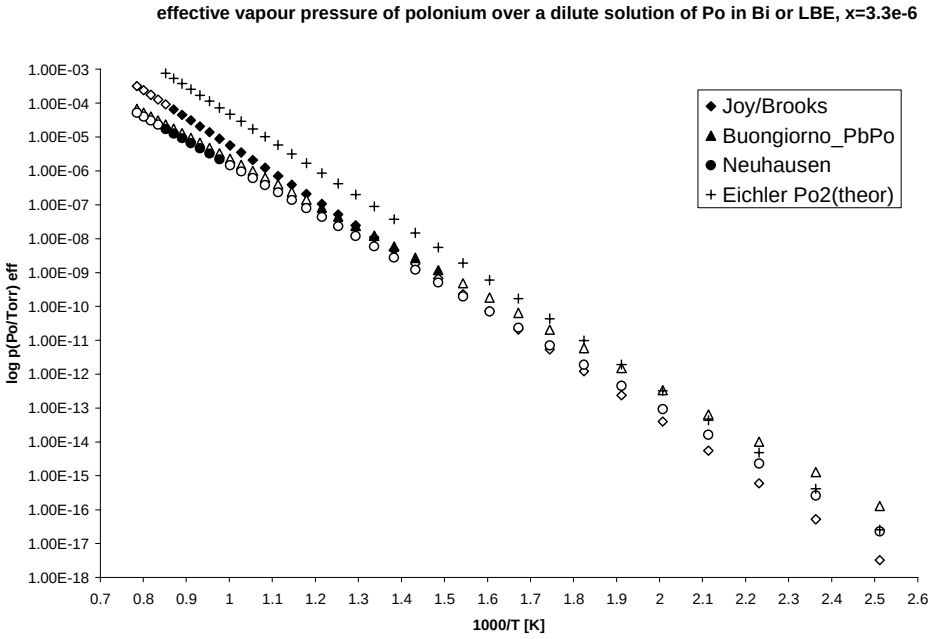

Eq. (5.26) was used to calculate the vapour pressure of polonium above a solution with a mole fraction of $3.3*10^{-6}$ for polonium in liquid bismuth. The corresponding values are shown as diamonds in Figure 5.3.1. We assume that the chemical interactions of polonium with liquid bismuth and LBE are similar. Hence, the thermodynamic activity coefficients should be of a comparable magnitude and the results can be used for an evaluation of polonium in LBE.

[Buongiorno, 2003] studied the equilibrium vapour pressure of polonium over LBE ($x \approx 10^{-8}$) in the temperature range from 665 to 823 K in an argon atmosphere. They obtained the following vapour pressure relation as a function of temperature:

$$\log p_{Po(eff)}[\text{Torr}] = -6790/T[\text{K}] + 6.64 \qquad (5.30)$$

In this equation, an error introduced by the incorrect calculation of mole fraction values by the authors has been corrected. Since this equation corresponds to an effective vapour pressure over an LBE solution of polonium, where the thermodynamic activity coefficient is already included, we can calculate the vapour pressure for MEGAPIE conditions by multiplying the vapour pressure obtained using Eq. (5.30) with the mole fraction of $3.3*10^{-6}$ expected at the end of irradiation. The resulting values are plotted as triangles in Figure 5.3.1.

The release of polonium from liquid LBE has been studied at PSI under an $Ar/7\%H_2$ atmosphere as a function of temperature using carrier free amounts of polonium ($x \approx 10^{-12}$) [Neuhausen, 2004]. In these experiments the amount of polonium transported from a LBE sample under a constant gas flow during a constant time was determined (see Section 5.3.2). Evaluating the amount of polonium transported, an effective vapour pressure of polonium can be estimated using the perfect gas law. The

relation for this effective vapour pressure of polonium over liquid LBE derived from the results of release experiments between 1011 and 1167 K is given in Eq. (5.31):

$$\log p_{Po(eff)}\,[\text{Torr}] = -7158/T\,[\text{K}] + 6.82 \qquad (5.31)$$

By multiplying with the mole fraction expected for MEGAPIE we arrive at the values plotted as circles in Figure 5.3.1.

Eichler derived a consistent set of thermodynamic data for polonium (enthalpy, entropy, Gibbs energy) from extrapolations within the chalcogen group (see Section 5.2.1) [Eichler, 2002]. Based on these data, temperature functions for the vapour pressure of polonium have been derived for the evaporation of monoatomic polonium as well as diatomic Po_2 molecules. According to these data, Po_2 molecules should be the dominating species over pure polonium at temperatures relevant to MEGAPIE. For this reason we include in Figure 5.3.1 the vapour pressure of Po_2 over a solution with a mole fraction of $3.3*10^{-6}$ calculated from the vapour pressure function derived from thermodynamic functions [Eichler, 2002] and an estimation for the thermodynamic activity coefficient. The thermodynamic activity coefficient can be calculated from the following relation:

$$\Delta\overline{G}_{ex}\,(\text{Po in M}) = RT\ln\gamma \qquad (5.32)$$

where $\Delta\overline{G}_{ex}$ (Po in M) is the partial molar excess Gibbs free energy for the solution of polonium in a liquid metal, and:

$$\Delta\overline{G}_{ex}\,(\text{Po in Pb}) = \Delta\overline{H}_{ex}\,(\text{Po in M}) - T\Delta\overline{S}_{ex}\,(\text{Po in M}) \qquad (5.33)$$

where $\Delta\overline{H}_{ex}$ and $\Delta\overline{S}_{ex}$ are the corresponding excess enthalpies and entropies. While $\overline{S}_{ex}$ is not known, $\Delta\overline{H}_{ex}$ corresponds to the partial molar enthalpy of solution of polonium in liquid metals. The latter has been calculated in [Neuhausen, 2003] using the Miedema model. As a first approximation we use $\Delta\overline{H}_{ex}$ as an approximation for $\Delta\overline{G}_{ex}$ and neglect its temperature dependency. Based on Eq. (5.29) and the value of -10.2 kJ/mol for $\Delta\overline{H}_{ex}$ for polonium in liquid lead [Neuhausen, 2003] we obtain an activity coefficient of $\gamma = 0.016$ at 298 K.

For Po_2 over pure liquid polonium, the following vapour pressure relation has been obtained from extrapolated thermodynamic data [Eichler, 2002]:

$$\log p_{Po2}\,[\text{Torr}] = -7584.1/T\,[\text{K}] + 9.2795 \qquad (5.34)$$

Together with the values of mole fraction $x = 3.3*10^{-6}$ and activity coefficients calculated using Eq. (5.32) we calculate effective vapour pressures displayed as crosses in Figure 5.3.1.

The four curves show satisfactory agreement. This is valid especially in the temperature range between 1000 and 600 K. For a conservative assessment of polonium release we choose Eq. (5.30) because it gives the highest values for polonium vapour phase concentrations in the temperature region of interest for MEGAPIE.

An increase of polonium gas phase concentration has been observed when a mixture of hydrogen and water is bubbled through LBE [Buongiorno, 2003]. This effect has been attributed to the formation of polonium hydride, H_2Po. The experimental results were interpreted in terms of values for the Gibbs free energy change ΔG for the following reactions:

$$PbPo(s) + H_2O(g) \leftrightarrow H_2Po(g) + PbO \quad (5.35)$$

$$\Delta G\ [kJmol^{-1}] = (17.0 \pm 4.1) + (0.150 \pm 0.007) * T[K] \quad (5.36)$$

and:

$$H_2 + PbPo \leftrightarrow H_2Po + Pb \quad (5.37)$$

$$\Delta G\ [kJmol^{-1}] = -(7.90 \pm 4.1) + (0.103 \pm 0.007) * T\ [K] \quad (5.38)$$

From these relations, the gas phase concentration of H_2Po can be calculated using the relation between ΔG and the equilibrium constant K:

$$\Delta G = -RTlnK \quad (5.39)$$

where:

$$K = cPbO * cH_2Po / (cPbPo * cH_2O) \text{ for reaction} \quad (5.40)$$

and:

$$K = cH_2Po * cPb / (cH_2 * cPbPo) \text{ for reaction} \quad (5.41)$$

concentrations c are given in mol/l for all components and phases in [Buongiorno, 2003] and thermodynamic activity coefficients have been set as 1.

For reaction (5.35) we obtain:

$$c(H_2Po) = K * c(H_2O) * c_{PbPo}/c_{PbO} \quad (5.42)$$

and for reaction (5.37):

$$c(H_2Po) = K * c(H_2) * c_{PbPo}/c_{Pb} \quad (5.43)$$

The temperature functions for ΔG given in [Buongiorno, 2003] disagree with thermodynamic data for H_2Po and PbPo derived in an extrapolative manner using the periodicity within the chalcogen group [Eichler, 2004a]. The latter are in reasonable agreement with formation energies of H_2Po and PbPo calculated using quantum mechanical methods [Mavridis, 2005], [Neuhausen, 2003] and would give rise to much lower H_2Po gas phase concentrations. On the contrary, the formation of H_2Po has been reported by other groups [Pankratov, 1999 and references cited therein]. However, H_2Po is reported to be unstable in humid air. A 94% decay of H_2Po in humid air at 289 K was reported in [Pankratov, 1999]. Overall, the knowledge concerning formation and stability of H_2Po is not sufficient for a reliable evaluation of its importance for polonium release from LBE. For example, the higher gas phase concentrations of polonium observed in [Buongiorno, 2003] could also originate from the formation of LBE aerosols carrying polonium activity. Further study is necessary to clarify the situation.

5.3.1.2 Evaporation characteristics of polonium and its lighter homologues selenium and tellurium from liquid Pb-Bi eutecticum

Gamma-active isotopes of polonium and its lighter homologues selenium and tellurium were implanted into LBE samples at CERN-ISOLDE [Neuhausen, 2004]. The evaporation behaviour of

these elements dissolved in liquid LBE has been studied at various temperatures in the range from 482 K up to 1330 K under a continuous flow of Ar/H_2 or Ar/H_2O using γ-ray spectroscopy.

Polonium release in the temperature range of interest for technical applications is slow. Within short term (1 h) experiments measurable amounts of polonium are evaporated only at temperatures above 973 K as is shown in Figure 5.3.2. Long term experiments reveal that a slow evaporation of polonium occurs at temperatures around 873 K resulting in a fractional polonium loss of the melt of around 1% per day as shown in Figure 5.3.3. Evaporation rates of selenium and tellurium are smaller than those of polonium. The presence of H_2O does not enhance the evaporation within the error limits of experiments as illustrated in Figure 5.3.4. The thermodynamics and possible reaction pathways involved in polonium release from LBE are discussed in more detail in [Neuhausen, 2004] and [Eichler, 2004a].

Figure 5.3.2. Comparison of the release behaviour of selenium, tellurium and polonium from LBE (1 h experiments) in an Ar/7%-H_2 atmosphere as a function of temperature

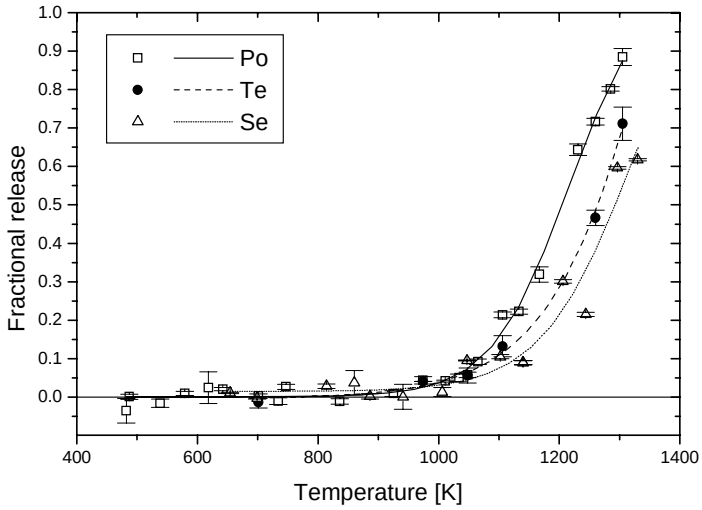

Figure 5.3.3. Comparison of the long-term polonium release from LBE in an Ar/7%-H_2 atmosphere at different temperatures as a function of heating time

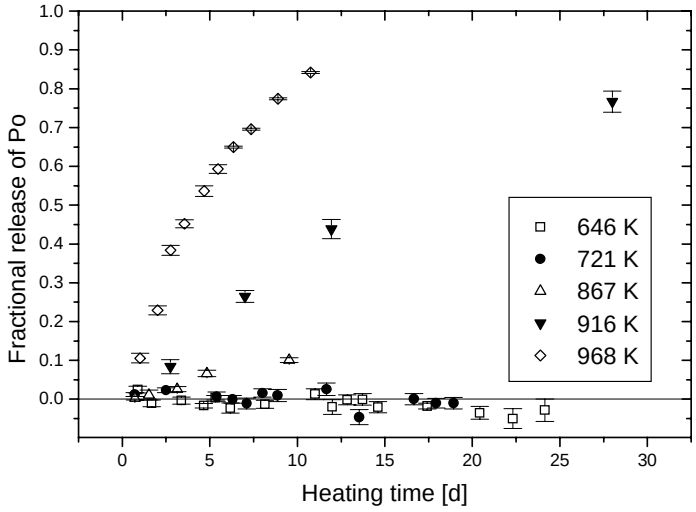

Figure 5.3.4. Comparison of the release of polonium from LBE (1 h experiments) in Ar/7%-H_2 and water saturated Ar atmospheres as a function of temperature

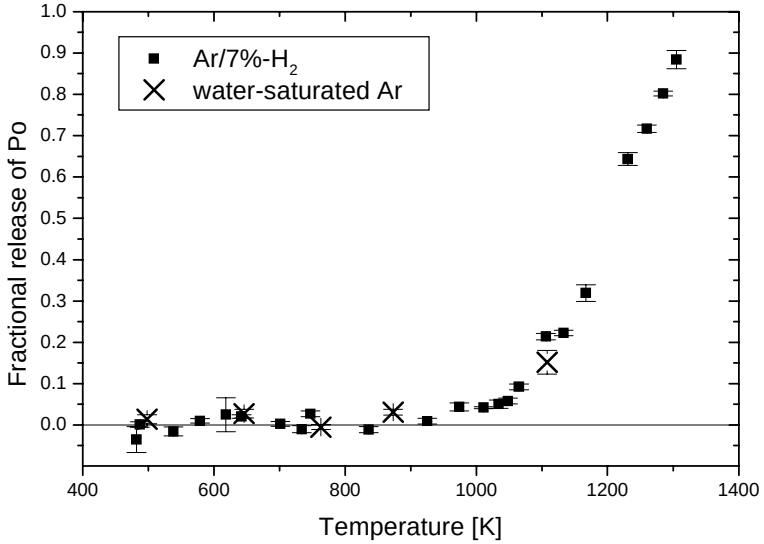

5.3.2 Thermal release behaviour of mercury and thallium from liquid eutectic lead-bismuth alloy

LBE samples have been irradiated with neutrons in SINQ at PSI, where mercury and thallium nuclides are formed by (n,xn) reactions of the sample materials and subsequent electron capture or β+ decay of Pb and Bi nuclides as well as (n,α) reactions [Neuhausen, 2005a].

The release of mercury and thallium from liquid LBE under a flowing Ar/7%-H_2 atmosphere has been studied in the temperature range from 408 to 1292 K using γ-ray spectroscopy [Neuhausen, 2005a]. For technical applications such as liquid metal spallation targets or accelerator-driven systems, where liquid LBE is planned to be used as the target material, the release of radioactive mercury isotopes produced by spallation is expected to be one of the major safety issues.

During short-term experiments, significant amounts of mercury begin to evaporate from liquid LBE at temperatures starting from about 475 K as shown in Figure 5.3.5. 80% of the mercury present in the sample is released from samples of approximately 1.5-3 g within one hour at temperatures higher than 625 K. Thallium release in the temperature range investigated is below experimental error. Long-term experiments reveal that even at temperatures as low as 476 K about 25% of the mercury present in the samples is released per day under a flowing Ar/7%-H_2 atmosphere as shown in Figure 5.3.6.

Further studies of Hg release were conducted using realistic concentrations of Hg and various gas atmospheres ranging from reducing to oxidising conditions [Neuhausen, 2006]. The main results are depicted in Figure 5.3.7. Under reducing conditions, substantial release of mercury from LBE starts at temperatures around 473 K. At about 571 K, half of the mercury present in the samples is released within one hour. The good agreement between results for carrier-free (mole fraction $\approx 10^{-12}$) and higher concentration (mole fraction $\approx 6*10^{-5}$) samples suggest that Henry's law is valid for the behaviour of Hg in LBE within this concentration range.

Figure 5.3.5. Fractional release of mercury and thallium from LBE (1 h experiments) in Ar/7%-H_2 atmosphere as a function of temperature

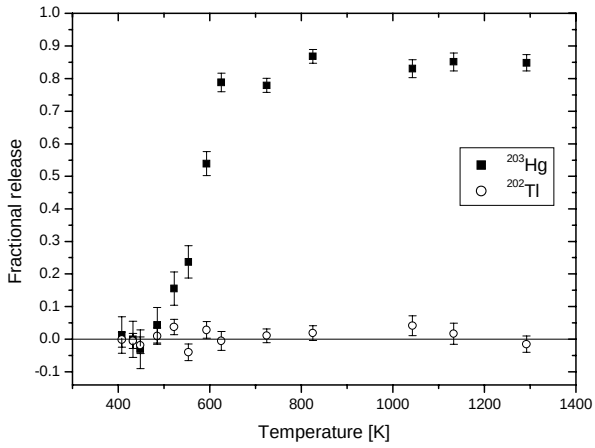

Figure 5.3.6. Comparison of the long-term mercury and thallium release from LBE in an Ar/7%-H_2 atmosphere at different temperatures as a function of the square root of heating time

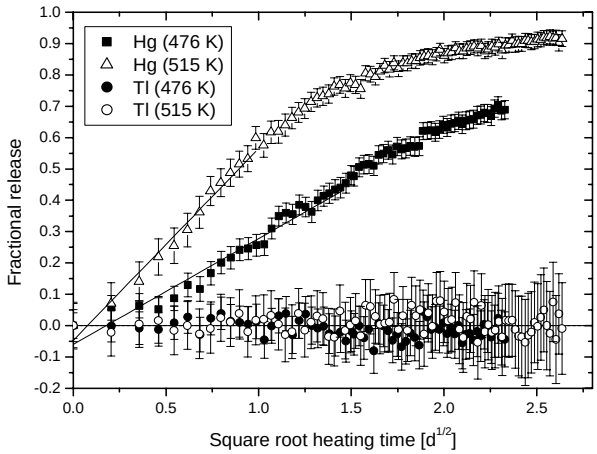

Figure 5.3.7. Comparison of the fractional release of Hg from liquid LBE under different gas atmospheres and different Hg concentrations

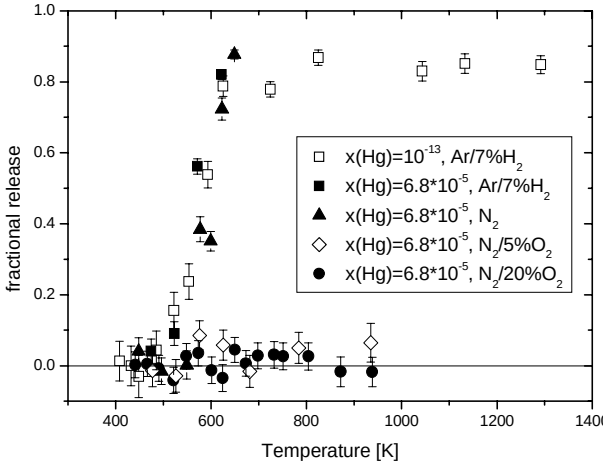

Oxidising conditions lead to a strong decrease of mercury release. In 1 h experiments, no release of mercury is observed for temperatures up to 935 K within the limits of experimental error when humid air is used as carrier gas. Apparently, the formation of an oxide layer on the surface of the melt inhibits the evaporation of Hg. This effect is of importance with respect to accident scenarios in liquid metal spallation targets, where liquid LBE could be exposed to air as well as cooling water. In such a case, a substantial decrease of the evaporation rate of mercury can be expected due to the formation of an oxide layer.

The use of noble metal absorbers for the fixation of mercury released to the gas phase has been examined in a preliminary study [Eichler, 2004b].

5.3.3 Release of volatile radionuclides in abnormal operating conditions

Different accident scenarios have been considered to estimate the hazards of a failure during the operation of a liquid metal system [Perret, 2002]. Many of these scenarios have a common feature: A surface of hot LBE will be exposed to an atmosphere containing oxygen and possibly water vapour from the evaporation of cooling water, which also can leak from the target system in case of a failure. Volatiles will be evaporated from the hot LBE surfaces to the target containment until LBE is solidified. A fraction of these volatiles may be released to the environment in case an interlinkage between the target containment and the environment is formed during the accident. The oxygen in the atmosphere will have an influence on the release behaviour. First of all, lead and bismuth oxides will form on the surface of LBE. This surface oxide layer can drastically decrease the release rate. Furthermore, the presence of oxygen shifts the hydrogen/water equilibrium ($H_2 + 1/2\ O_2 \leftrightarrow H_2O$) to the product side. Thus, release reactions that involve hydrogen containing volatile species, e.g. H_2Po, will be suppressed.

In this section, a simple general procedure to estimate the maximum release of volatiles from a given LBE surface is shown. Parameters like the area of the LBE surface as well as its temperature as a function of time have to be specified. This approach only considers the maximum amount of volatiles to be released from such an LBE surface. The fraction of these volatiles that will be finally transported to the environment is not considered.

The following equation for the maximum evaporation rate of a metal into vacuum was derived by Langmuir from kinetic gas theory [Langmuir, 1913]:

$$R_m = 0.0583 * p^\circ * \sqrt{M / T} \tag{5.44}$$

where R_m is the evaporation rate [$gcm^{-2}s^{-1}$], p is the vapour pressure of pure metal [Torr] and M is the atomic/molecular Mass [$gmol^{-1}$].

Evaporation rates observed in practice under non-vacuum conditions typically are considerably lower [McNeese, 1967] due to collisions of the evaporating particles with molecules of the gas phase.

For a component A in a dilute mixture, the vapour pressure of the pure metal is replaced by its vapour pressure over the dilute solution

$$p_A = \gamma_A * x_A * p_A^\circ \tag{5.45}$$

where p_A is the vapour pressure of the component A over the mixture [Torr], x_A is the mole fraction of the dissolved component A, γ_A is the thermodynamic activity coefficient of the dissolved component A and p_A is the vapour pressure of the pure component A [Torr].

Hence:

$$R_{mA} = 0.0583 * \gamma_A * x_A * p_A^{\circ} * \sqrt{M / T} \quad [gcm^{-2}s^{-1}] \tag{5.46}$$

As a conservative approach, it is recommended that Eq. (5.46) be used to assess the evaporation of volatiles for accident scenarios in cases where experimental data on release rates are not available.

For mercury [Greene] and polonium [Tupper, 1991] experimental investigations on release rate have been performed. The results of these investigations can be used to assess the release of these two most important volatiles. A quantitative evaluation [Neuhausen, 2005b] of polonium release experiments performed at PSI [Neuhausen, 2004] confirmed the release rates measured in [Tupper, 1991]. These data are plotted in Figure 5.3.8. From these evaluations, the following temperature function for the release rate of polonium was derived:

$$\log R_m/x = 0.97 \pm 0.22 - 6049 \pm 200/T \tag{5.47}$$

with a correlation coefficient of 0.99352, and where R_m is the mass release rate of polonium [$gcm^{-2}s^{-1}$], x is the mole fraction of polonium and T is the temperature in K.

This function can be used for the calculation of evaporation rates under various accident scenarios.

Figure 5.3.8. Comparison of Po release rate from liquid LBE normalised to Po mole fraction measured in different experiments [Neuhausen, 2005b]

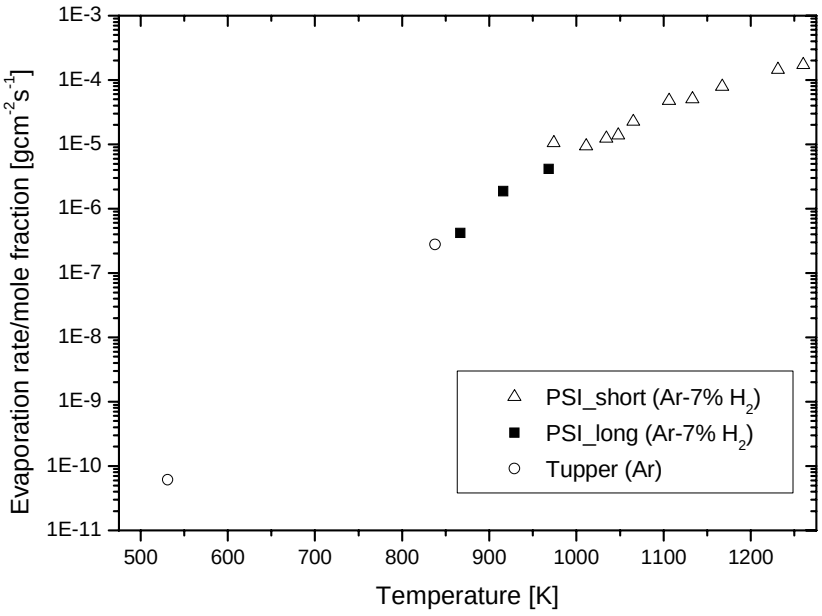

A preliminary study of polonium removal from contaminated quartz plates is described in [Obara, 2003]. Contamination of quartz plates was achieved by deposition of Po-contaminated LBE evaporated at approximately 1273 K. The deposition took place at about 873 K under an argon atmosphere. Polonium was selectively removed from the quartz plates in vacuum at 573 K, leaving the non-radioactive fraction of the deposited material on the quartz surface.

5.4 Irradiation effects

5.4.1 Measurement of gas and volatile element production rates in a proton-irradiated molten lead-bismuth target in the ISOLDE facility

5.4.1.1 ISOLDE facility and proton beam

A knowledge of the production rate and of the release properties of stable and radioactive volatile elements produced during operation of a spallation target is essential. A liquid spallation target comprises new design challenges which must be faced in view of the construction of a full-scale ADS prototype. One of the aspects that must be considered in the design of the MEGAPIE target is how to handle the gas produced during operation. Following the interaction of the high-energy proton beam with the target, nuclides are produced, many of which have high volatility. As an indication, a list of elements with high volatility is given in [Köster, 2001]. The elements are classified on the basis of the temperature at which the vapor pressure reaches 0.01 mbar. The products with high volatility are H, He, N, O, F, Ne, Cl, Ar, Br, Kr, I, Xe, Hg and At. The products with lower volatility, but still significant at the operating temperatures of the MEGAPIE experiment, are Na, P, S, K, Zn, As, Se, Rb, Cd, Te, Cs, and Po.

An experiment was conducted to study the production rates of stable and radioactive volatile elements in a LBE target irradiated by a proton beam of the energy of the order of 1 GeV. In this section the experiment is described and initial results are shown.

The experiment was performed at the ISOLDE facility [Kugler, 2000]. A schematic view is shown in Figure 5.4.1. The facility is connected to the PS booster (PSB), consisting of four small synchrotrons. Protons from a linac are pre-accelerated to 1 GeV or 1.4 GeV, before being injected to the 27 GeV proton synchrotron.

Figure 5.4.1. Schematic view of ISOLDE hall

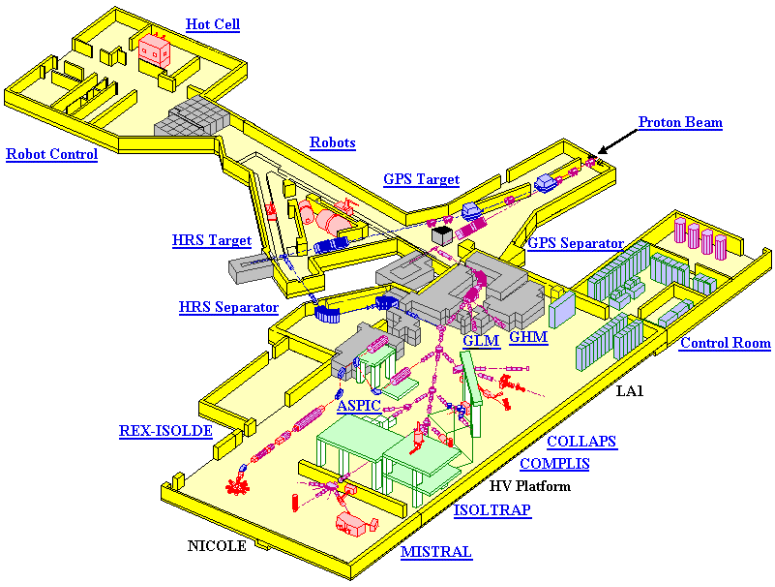

The PSB provides one pulse of $3.2 \cdot 10^{13}$ protons every 1.2 seconds. A supercycle is made up of a string of 12 pulses. Up to half of the pulses in a super cycle can be delivered to the ISOLDE target. The protons from the PS Booster are delivered to the targets via a 100 m long underground transfer

line. The proton beam is sent either to the High Resolution Separator (HRS) target or to the General Purpose Separator (GPS) target. The proton beam energy in the experiment was of 1.4 GeV. In the experiment one pulse per super cycle (16.8 s) was used. Proton pulses of 1.4 GeV and variable intensity (up to 10^{13} protons/pulse with a rate of one pulse every 16.8 s) impinged on the target. Following the spallation reactions, the volatile elements produced and exiting the liquid metal were ionised by means of a plasma ion source, then accelerated to 60 keV and sent to the magnetic mass separators and to the beam lines where the measuring stations were located.

5.4.1.2 ISOLDE target

The spallation targets at ISOLDE are contained in special target units. Cylindrical tantalum containers, 20 cm long and with 1 cm radius, are filled with the target material. Tantalum is a heavy, hard and ductile metal most unlikely to react with most elements and with a high boiling point.

The target material was a LBE sample with mass of 547 grams. The measurements were performed with the target at temperatures of 400°C and 600°C. Temperature differences within these ranges are not expected to affect the releases of the noble gases and Hg isotopes. On the other hand, differences are expected for some isotopes such as I, Cd and Po.

Table 5.4.1 presents the parameters of the beam and target for the experiment.

Table 5.4.1. Summary of beam and target parameters for the ISOLDE experiment

Parameter	ISOLDE experiment
Beam energy	1.4 GeV
Beam pulse length	2.4 μs
Beam repetition rate	16.8 s
Beam current (average value)	$0.95 \cdot 10^{-4}$ mA (for 10^{13} ppp)
Beam profile (Gaussian)	$\sigma_x = \sigma_y = 3.5$ mm
LBE mass	547 g
Target size (cylindrical)	L = 20 cm, r = 1 cm
Target temperature at experiment	400°C, 600°C
Transfer line temperature	300°C

5.4.1.3 Measurement techniques

Yields were measured using three different techniques in common use at ISOLDE.

1) Online yields of stable as well as some radioactive isotopes were measured using a Faraday cup (FC) inserted in the beam line. A special data acquisition system was developed at PSI [Manfrin, 2004] to trigger the current measurement with the arrival of the proton beam on target, thus allowing the measurement of the gas release curves, characteristic of each element.

2) For short-lived β emitting isotopes, beams were directed to a dedicated tape station and yields were measured with a plastic scintillator detector. The online measurement with the tape station allows correction for partial decay of isotopes produced inside the target, before the release. In fact, since the release is dependent on the chemical properties of a given element, it is possible for instance to fit the release functions of ^{6}He (measured with the tape station) and ^{4}He (measured with the Faraday cup) and correct for the partial decay of the ^{6}He.

3) A third measurement method was used for longer-lived ($T_{1/2} \geq 5$ min) γ-emitting radioisotopes; ion beams were implanted on thin Al foils at the measuring station, then after irradiation an offline γ detection was performed using a calibrated HPGe detector.

5.4.1.4 Data analysis

The release process of volatile elements

The release of the volatile elements from a molten metal target is a complex process [Köster, 2000]. The volatile species formed in the interaction process first diffuse in the liquid. The *diffusion* rates in the bulk material depend on the temperature and on the atomic mass. Following diffusion through the bulk material, the elements diffuse through the target container, the transfer line and the ion source. The *effusion* time is given by the number of wall collisions times the average time between two wall collisions. For a real target/ion source combination the total release time is given by a combination of the diffusion time and the effusion time.

The average release time for a volatile product from a liquid target is typically in the order of minutes, and decreases with increasing temperature.

The release profiles are typically described by a sum of two exponential decay terms multiplied by an exponential grow-in term as follows from [Köster, 2000]:

$$p(t) = C\left(1 - \exp\left(-t/\tau_r\right)\right)\left[\alpha\, exp\left(-t/\tau_f\right) + \left(1-\alpha\right) exp\left(-t/\tau_s\right)\right] \tag{5.48}$$

where τ_r is the characteristic rise time, τ_f and τ_s are two decay times, fast and slow; α is the relative contribution of the fast and slow components and C is a normalisation factor.

Almost all elements in these experiments are released with a fast peak component shorter than 6 seconds and a slow peak at longer times. Figures 5.4.2 and 5.4.3 show the release curves for ^{80}Kr and ^{196}Hg measured with the Faraday cup. The fast part of the release curve is easily identified as the peaks in the beginning of the curve. The small drop just before the big peak is a result of the fact that the high voltage supply is pulsed (to avoid possible break down following the beam impact), and is brought to zero 35 μs before beam impact, and then restored to the regular 60 kV value after 5 ms [Kugler, 2000].

Figure 5.4.2. ^{80}Kr release function, measured with the LBE target at proton beam intensity of 1×10^{13} protons/pulse, during 6 seconds

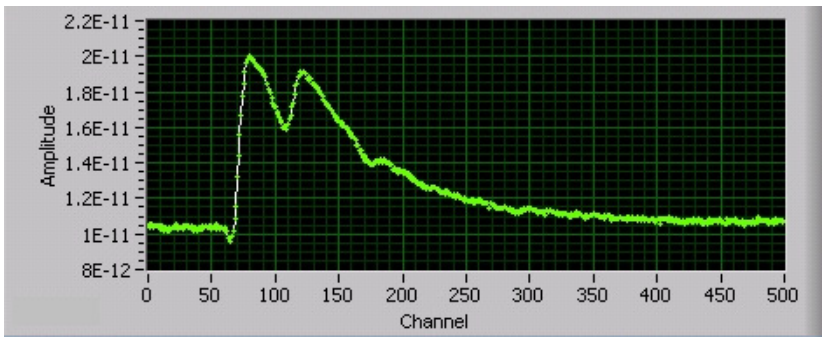

Figure 5.4.3. Same as Figure 5.4.2 but for ^{196}Hg

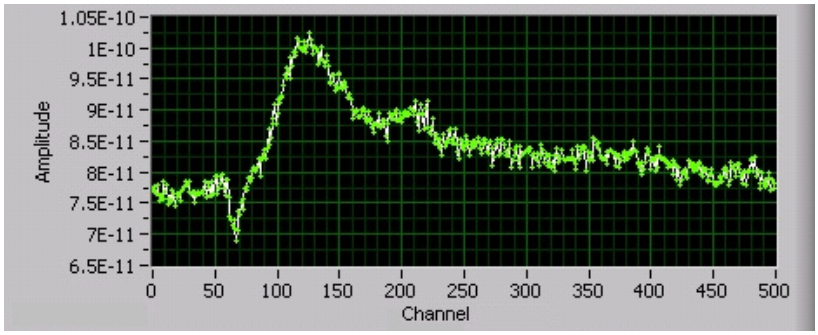

The tail after the peak represents the slow component of the release function. The tail of the release function is longer than the cycle length of 16.8 seconds, and therefore the long components of the release function accumulate one on top of another, forming a background level that can be observed at the left of the main peak. Thus in order to measure the whole release one has to measure for an entire cycle length.

The drop in the middle of ^{80}Kr release peak was probably due to fluctuations in the efficiency of the plasma ionisation source because of the pulsed beam. This is an effect that is dependent on the proton beam intensity. As far as its effect on determination of the production rate goes, this drop is not significant since the total release is dominated by the slow component.

The study of release functions is important for very short lived isotopes, like ^{6}He. By comparing the release functions of ^{6}He (measured with the tape station) and ^{4}He (measured with the Faraday cup) the fraction of the decay of ^{6}He before detection can be calculated.

Efficiency

The rate of particles detected *r* can be described by the following relation [Köster, 2000]:

$$r = \Phi\, \sigma_{ind} N \varepsilon_{rel}\, \varepsilon_{ion} \varepsilon_t\, \varepsilon_{det} \tag{5.49}$$

where the Φ is the flux of the incident particles, the protons, σ_{ind} the cross-section for producing a given isotope in the target and *N* the number of target atoms exposed to the incident beam. Decay losses are included in all the efficiencies, and are only relevant for short-lived isotopes. One should note that the individual efficiencies correlate. For example if the efficiency of an ion source is improved, the emittance may worsen, thus reducing the transmission efficiency [Köster, 2000]. The release efficiency, ε_{rel} is the fraction of the isotope that is released from the target after the spallation reaction. It is equal to one for the off-line results and plays only a role in the short-lived isotope measurements done with the tape station. All measured isotopes in the off-line measurements have half-lives long enough for not influencing the release efficiency.

The ionisation efficiency, ε_{ion} is the fraction of the released isotopes that are really ionised, in the ion source. The ionisation efficiency is in fact a product of three different efficiencies: the ionisation efficiency, the extraction efficiency and the separator efficiency, but in this experiment they are considered as one unit. The transmission efficiency, ε_t i.e. the fraction of the released and ionised isotopes that are transported to the measuring station. *The detector efficiency*, ε_{det} i.e. the fraction of the emitting γ-rays (in the case of the γ-spectroscopy measurement) or β-radiation (in case of the tape station measurement) which are detected.

In order to obtain the absolute production rates from the measured yields, the efficiency of the ion source had to be measured. For this purpose, known amounts of different gas mixtures (consisting of Ar/Xe and He/Ne/Kr/Xe) were leaked into the ion source, allowing measurement of the efficiencies at any time during the experiment. For the other elements, the ion source efficiency was deduced (with somewhat larger errors) from the dependence on the ionisation potential and the mass of the isotopes, or from existing data in the literature. In the first test the ion source was injected with a mixture of 95% Ar and 5% Xe at 0.922 bar and in the second test it was filled with a mixture of 40% He, 20% Ne, 20% Kr and 20% Xe at 1.00 bar. A difference of about 30% between the two measurements indicates a probable small leakage of the ion source. Measured ionisation efficiencies for xenon were about 3.7 %. The ionisation efficiency for mercury cannot be measured but results in [Kirchner, 1996] show an ionisation ratio of about a factor 1.5 for Hg+/Xe+. Using this ratio, we assumed an ionisation efficiency of 5.5 % for Hg.

Additional corrections are needed for radioactive isotopes to account for their decay between the production time at the target and the detection time. The corrections are different for the tape station and the collection measurements. In this discussion we concentrate on the latter case, as well as on the Faraday cup measurement, for which no corrections are necessary since stable or long-lived isotopes are measured with this technique.

In most of the cases, a given nuclide can be formed not only by production following a spallation reaction, but also by the β decay of other isobaric nuclei, or by α decay. In this case what is measured is the *cumulative* cross-section, that is, the sum of the *independent* cross-section plus the contribution from the decaying parents. This contribution is usually very important. Ideally, the measurement should start when the contribution from decaying parents has reached a constant level (equilibrium conditions), so that the comparison with calculated values is easier. During the measurement, this was the case for most of the isotopes, with some exceptions especially for Hg isotopes.

Different transmission lines in the ISOLDE facility were used for the off-line and the on-line measurements. The *transmission efficiency* is about 90-95% for the off-line collection as well as for the FC and slightly lower, 88%, for the tape station.

Monte Carlo calculations

The Monte Carlo calculations were done using the codes FLUKA [Fasso, 2001] and MCNPX [Waters, 2002]. A simple model of the LBE target was used, as shown in Figure 5.4.4. A cylinder filled to 75% with LBE and bombarded by a 1.4 GeV proton beam was modelled. Although the geometry of the target is more complex, this simple modelling should be accurate enough to provide expected production rates. In fact, the target material is surrounded by the structure of the target holder, consisting essentially of Al and Cu. No difference should be expected by introducing these extra elements, as they are not moderating materials. The only moderating material is placed about 1 m away from the target, and is the marble beam dump. The isotope production rate in the target was calculated in atoms/μC.

Figure 5.4.4. Calculation model used in the Monte Carlo programs

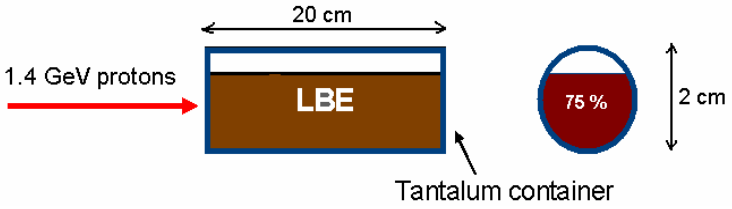

For the MCNPX calculations, different model options for the spallation reaction and evaporation were used, as discussed below. By using the additional codes ORIHET3 [Atchison, 2001] and FP-FISPACT [Petrovich, 2001] the cumulative production rates were calculated.

As an example, in Figure 5.4.5 the calculated build-up of ^{127}Cs as a function of the time after start of irradiation is shown. This isotope decays to ^{127}Xe with a half-life of 6.25 h, thus contributing to the production of this isotope. In this case after about one day an equilibrium condition is reached, where the amount of ^{127}Cs is constant.

Figure 5.4.5. Calculated build-up of ^{127}Cs after start of irradiation. In this case equilibrium conditions are reached after about two days.

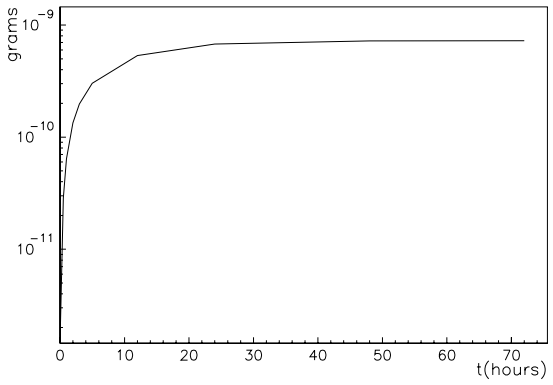

Measured isotopes

Collection measurements were performed for a number of isotopes. These include the release of He, Ne, Ar, Br, Kr, I, Xe, Hg, Po, and At radioisotopes.

During the first measurement run more attention was concentrated on those isotopes which are critical for the operation of an ADS target.

Offline γ spectroscopy can be applied if the half-life of the isotope is longer than 10-15 minutes (the time it takes to get the sample to the germanium detector and begin the analysis with the acquisition program). Theoretically there is no upper limit in half-life, but to get good statistics one should choose isotopes with half-life less than some days or weeks, depending on the activity of the isotope.

5.4.1.5 First results

Mercury

Production of mercury isotopes is important as they are expected to contribute a significant part of the total radiotoxicity during operation of an LBE target.

Figure 5.4.6 presents the measured cumulative production rates for radioactive Hg isotopes. Longer–lived Hg isotopes are expected to be completely released at a temperature of 600°C. The ionisation efficiency was not measured for Hg, as it was only measured for noble gases. As discussed above, an efficiency of a factor 1.5 higher than the measured Xe efficiency of 3.7% was assumed.

Figure 5.4.6. Production rates for Hg isotopes

Measured points (black squares) are compared with calculations:
open circles – MCNPX (Bertini/Dresner model combination); diamonds – MCNPX (INCL4/ABLA); stars – FLUKA

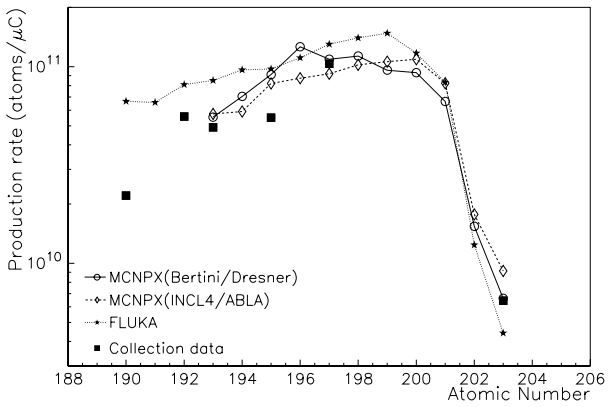

The measured values are in line with expected cumulative production rates calculated using FLUKA and MCNPX. The two codes were coupled with the evolution codes ORIHET3 and SP-FISPACT, respectively. In the case of MCNPX, results are shown here with two different model combinations for the intranuclear cascade and evaporation models. The circles represent results from using the Bertini intranuclear cascade model with the Dresner evaporation code. The diamonds are obtained using the recently implemented INCL4/ABLA [Boudard, 2002] model combination. The trend observed in the data as a function of atomic mass is reasonably well reproduced by the three calculations. One should note that for ^{193}Hg, ^{195}Hg and ^{197}Hg, there are isomeric states of 11.1 h, 40 h and 23.8 h half-lives, respectively. For these three isotopes, equilibrium was not achieved between formation and decay of the respective isomeric states, and the data are not corrected for this effect. Overall these results confirm the expected production rates of Hg isotopes in a thick LBE target.

In Figure 5.4.7 a comprehensive display of the experimental results for Hg isotopes obtained with the three techniques with the LBE target is shown. Data refer to measurement with the target at 400°C, with the exception of the collection data which were taken at 600°C. However, it is apparent from the figure that at the two temperatures the released fraction of long-lived isotopes is very similar.

Figure 5.4.7. Measured production rates for Hg isotopes from the Faraday cup (triangles), γ spectroscopy from collection data (squares), and β detection from the tape station (circles)

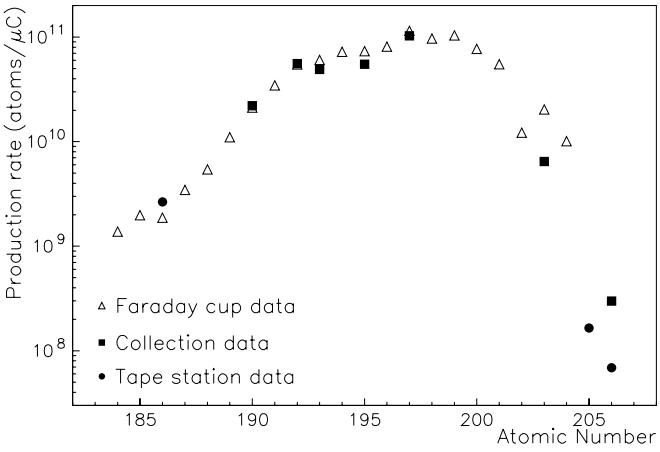

Xenon and iodine

Results for Xe isotopes, also measured with the LBE target at T = 600°C, are shown in Figure 5.4.8. In this case there is a clear disagreement between the values calculated with MCNPX with Bertini/Dresner, and the results from the other two calculations. The data, with an ionisation efficiency of 3.7% for Xe isotopes seem to favour the other two calculation results, thus confirming recent experimental findings [Enqvist, 2001].

Figure 5.4.8. Same as Figure 5.4.6 but for Xe isotopes

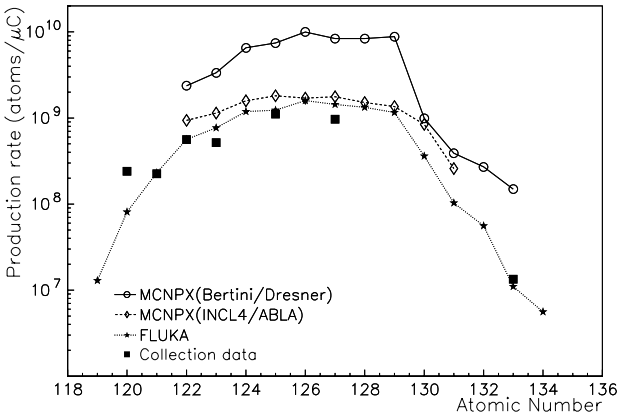

While production of Hg isotopes from a Pb/Bi target is due to direct spallation, the Xe and I isotopes are the results from a later stage of the spallation process, the fission of highly-excited spallation fragments, or as a two-step process due to neutron-induced fission from high-energy spallation neutrons. Thus the evaporation models, the Dresner and ABLA, are probably most responsible for the differences observed in the calculations.

Similar results as for Xe are obtained for the iodine isotopes. However, iodine is not completely released and observed production rates at 600°C are a factor 10 lower than the calculated FLUKA values.

Polonium and astatine

In an LBE target the build-up of Po is a very important. ^{210}Po is the isotope with the highest radiotoxicity among the volatile elements.

There are a number of possible reactions that can lead to astatine production. The dominating reaction is probably ^{209}Bi (p,π^- xn) $^{210-x}$At.

The calculated production rates of Po isotopes are of the order of 10^{10} atoms/μC. In the experiment, very small amounts of Po and At were observed. It was thus important to determine whether the observed Po came from At decay or it was indeed a release. By comparing the measured ^{207}Po production rates at different times with ^{207}At concentrations, it was concluded that even these small observed quantities are due to the decay of At and not to Po release. This is in agreement with other data [Neuhausen, 2004] which show that little or no release of Po is expected at temperatures of 600°C.

Helium

Production of He is of particular interest since this element, together with hydrogen represent the volatile elements produced in larger quantities during operation of a spallation target. The production rate for ^{4}He measured with the Faraday cup is about 0.33 atoms/p, with an uncertainty of about 30%. This value is in good agreement with calculations with MCNPX, which gives values of 0.4-0.8 atoms/p, depending on the model combination used.

Other isotopes

Of the other isotopes measured and analysed, no release of Br was observed, while very little amounts of Cd isotopes were detected.

5.4.1.6 Conclusions and outlook

The first analysis from the measurements of production rates of volatile elements from the irradiated LBE target gives results consistent with the expectations from Monte Carlo calculations. Overall, these preliminary results confirm the expected production rates in an ADS target.

5.4.2. Irradiation experiments

5.4.2.1 Pb and LBE irradiated in the STIP experiments using the Swiss Spallation Neutron Source (SINQ)

The Swiss Spallation Neutron Source (SINQ) is currently operated at 0.6 MW with a proton beam of 1.1 mA current with an energy of 550 MeV. The SINQ targets are composed of a matrix of lead (Pb) rods clad with AISI 316L tubes. The Pb rods are 9.8 mm in diameter and about 120 mm long. The cladding tubes are of 9.8 mm inner diameter and 10.8 mm outer diameter. With the end caps, the total length of a target rod is 136 mm. During irradiation the target rods are cooled by flowing heavy water. The beam has an approximately 2-D Gaussian distribution profile. The irradiation dose and temperature depends on the positions in the target.

The SINQ Target Irradiation Program (STIP) has been carried out to irradiate test specimens in SINQ targets since 1998. To date, three irradiation experiments were performed and a fourth experiment has been run in the present target but will not be reported here. In the second irradiation experiment, STIP-2, which was performed in 2000 and 2001, there were two rods containing test specimens in contact with LBE. For the post-irradiation examinations (PIE) of the STIP-2 specimens, the specimen rods and some selected normal target rods were transferred to the hot cells of PSI in 2003. In 2004, some LBE and Pb samples were obtained from one of the two LBE rods (R-B) and a normal target rod (R-Pb3) for PIE.

The Pb rod, designated R-Pb3, received the highest proton fluence in SINQ Target-4 where the STIP-2 experiment was performed. The maximum proton and neutron fluences received by this rod were 5.5×10^{25} p/m^2 and 9×10^{25} n/m^2. The maximum irradiation temperature was about 538 ± 30 K measured at the centre of the rod.

The maximum proton and neutron fluences of the LBE rod R-B were 4.7×10^{25} p/m^2 and 9.7×10^{25} n/m^2. The maximum irradiation temperature was about 633 ± 40 K. It is believed that most of LBE was melted during irradiation. However, due to test specimens inside the LBE, the LBE

should remain static. The rod was cut into four segments. Four small pieces of LBE were obtained from each segment after re-melting it in a hot cell at about 443 K. Due to the high activity of the small pieces, the γ-spectrometry and ICPMS analysis are expected to be done in 2006.

5.4.2.2 LBE irradiated in the LiSoR experiment

The LiSoR (**Li**quid metal – **So**lid metal **R**eaction) loop is a unique facility which was designed to investigate simultaneously the influence of flowing lead bismuth eutectic (LBE), static stress and irradiation by protons onto a specimen.

The loop with the test section was designed and constructed by Subatech, France; the liquid metal pump and flow meter was delivered from IPUL, Latvia; assembling, cabling, isolating and commissioning was performed at PSI, Switzerland. The LiSoR test facility installed in the IP1 bunker is connected to a beam line from the Philips PSI accelerator. The beam energy on the target was about 72 MeV maximum for the five irradiation experiments while different beam currents between 15 and 50 μA were chosen for each irradiation period.

The loop was fabricated of austenitic stainless steel 316L whereas in the test section ferritic steel T91 was used. The flow rate of the pump is up to 0.3 l/s, which corresponds to a flow velocity of about 1 m/s in the test section. The total amount of LBE in the melting vessel was about 18 l whereby approximately 15 l were filled into the loop for operation.

As of this date five LiSoR test sections have been irradiated. After each irradiation cycle the loop was drained and the irradiated LBE was collected in the storage tank together with the non-irradiated remaining 5 l. After a reasonable decay time the test section was disconnected from the loop and transported into a hot cell for dissembling and examination. LBE was never changed or refilled, i.e. most of LBE was irradiated during all the experiments except that remaining in the storage tank. The isotopes generated during irradiation are mostly short-lived nuclides with half-life times in the range days at most. Only the isotopes ^{207}Bi ($T_{1/2}$ = 32.2 y) and ^{208}Po ($T_{1/2}$ = 2.898 y) have relatively long half-life times. The other isotopes except ^{207}Bi and ^{208}Po formed during the irradiation experiments 1 to 4 decayed. The time between irradiation experiment no. 4 (ended after only 144 h of irradiation on 25 June 2003) and no. 5 (irradiation started on 21 April 2004) was nearly 10 months, enough time for decay of the short-lived nuclides.

The eutectic Pb-55.5Bi (44.8 wt.% Pb and 55.2 wt.% Bi) alloy which was used for filling LiSoR was supplied by Impag AG, Switzerland and contained a very low concentration of impurities: Ag 11.4, Fe 0.78, Ni 0.42, Sn 13.3, Cd 2.89, Al 0.3, Cu 9.8 and Zn 0.2 ppm respectively. During the commissioning phase (app. 2000 h of operation with LBE temperatures between 473 and 573 K without irradiation) and during the five irradiation periods the level of impurities should have increased due to corrosion products (dissolving of steel elements) and formation of stable decay products.

The irradiated LBE after LiSoR 2 experiment was analysed with high-resolution α-spectroscopy on chemically separated solutions [Glasbrenner, 2005]. Additionally, calculations were made in order to compare them with the experimental results. In Table 5.4.1 the calculated values are compared with the experimental ones. The analysis was carried out about half a year after the irradiation was completed. Thus only Po isotopes could be analysed due to their relatively long half-life time. Calculations taking the correct beam parameters into account revealed the generation of the Po isotopes 202, 203, 204, 205 and 207. It is believed that theses isotopes were present during and directly after irradiation but due to their short half-life times they were already decayed when the analysis was started. A comparison of the calculated and the experimental activities achieved for the Po isotopes 206 and 208 shows a good

Table 5.4.1. Values of Po isotopes revealed by neutronic calculation in comparison with experimental data

Isotope	Bq/calc.	Bq/g calc	Bq/g exp
^{202}Po	$3.1 \cdot 10^{9}$	$1.6 \cdot 10^{4}$	
^{203}Po	$2.3 \cdot 10^{11}$	$1.2 \cdot 10^{6}$	
^{204}Po	$9.9 \cdot 10^{11}$	$5.3 \cdot 10^{6}$	
^{205}Po	$1.1 \cdot 10^{12}$	$5.9 \cdot 10^{6}$	
^{206}Po	$9.1 \cdot 10^{10}$	$4.8 \cdot 10^{5}$	$9.95 \cdot 10^{5}$
^{207}Po	$7.9 \cdot 10^{11}$	$4.2 \cdot 10^{6}$	
^{208}Po	$5.9 \cdot 10^{8}$	$3.1 \cdot 10^{3}$	$4.8 \cdot 10^{3}$
^{210}Po	$2.0 \cdot 10^{6}$	11	150

consistence of the values, whereas the estimation of the ^{210}Po activity is too low. The generation of the ^{210}Po isotope requires thermal neutrons and the FLUKA code has only included reactions with fast neutrons. It is definitely possible that during the irradiation a small amount of thermal neutrons are generated which are responsible for the formation of ^{210}Po. For future calculations the FLUKA code has to be modified or another tool has to be used for performing these calculations.

During dissembling of LiSoR test section No. 5 samples of irradiated LBE were taken out from different positions. All irradiated LBE samples were examined by the following techniques:

- γ-spectrometry of solid materials but also of dissolved LBE samples to detect nuclides decaying by gamma irradiation;
- α-spectrometry on special processed LBE samples to analyse the different Po isotopes;
- ICP-MS on dissolved LBE probes to analyse all elements present in the different LBE samples.

In parallel to the analytical examinations calculations will be carried out using the FLUKA Monte Carlo code to compare the different analytical results with the calculations.

REFERENCES

Abakumov, A.S., Z.V. Ershova (1974), "Vapor Tension of Polonium and Lead Polonide", *Radiokhimiya*, Vol. 16, pp. 397-401, *Soviet Radiochemistry*, Vol. 16, pp. 396-399.

Atchison, F., H. Schaal (2001), *ORIHET3 – Version 1.12, A Guide for Users*, March 2001.

Ausländer, J.S., I.I. Georgescu (1956), *Proc. 1st Int. Conf. Peaceful Uses Atomic Energy*, Geneva, 1955, Vol. 7, p. 389.

Barin, I. (1995), *Thermochemical Data of Pure Substances*, 3rd ed. Verlag Chemie, Weinheim.

Beamer, W.H., C.R. Maxwell (1946), *J. Chem. Phys.*, Vol. 14, p. 569.

de Boer, F.R., R. Boom, W.C.M. Mattens, A.R. Miedema, A.K. Niessen (1988), *Cohesion in Metals, Transition Metal Alloys*, North-Holland, Amsterdam.

Brewer, L. (1995), "Thermodynamic Properties of the Oxides and their Vaporization Processes**",** *Chem. Rev.*, Vol. 52, pp. 1-75.

Brooks, L.S. (1955), "The Vapour Pressure of Polonium", *J. Am. Chem. Soc.*, Vol. 77, p. 3211.

Boudard A., *et al*. (2002), "Intranuclear Cascade Model for a Comprehensive Description of Spallation Reaction Data"**,** *Phys. Rev. C*, Vol. 66, 044615-044666.

Buongiorno, J., C. Larson, K.R. Czerwinski (2003), "Speciation of Polonium Released from Molten Lead Bismuth", *Radiochim. Acta*, Vol. 91, pp. 153-158.

Eichler, B. (2002), *Die Flüchtigkeitseigenschaften des Poloniums*, PSI-Report Nr. 02-12, June 2002, ISSN 1019-0643.

Eichler, B., J. Neuhausen (2003), *Analyse der Thermochemischen Beziehungen des Iods in einem Blei-Wismut-Spallationstarget*, TM 18-03-01, Paul Scherrer Institut, Villigen, Switzerland, August 2003.

Eichler, B, J. Neuhausen (2004a), *Verflüchtigungspfade des Poloniums aus einem Pb-Bi-Spallationstarget (Thermochemische Kalkulation)*, PSI-Report Nr. 04-06, June 2004, ISSN 1019-0643.

Eichler, B., J. Neuhausen (2004b), *Radiochemische Untersuchung der Sorption und Desorption von Quecksilber an Silber*, Technical Note TM-18-04-01, Paul Scherrer Institut, July 2004.

Enqvist T., *et al*. (2001), "Isotopic Yields and Kinetic Energies of Primary Residues in a 1 A GeV ^{208}Pb+p Reactions", *Nucl. Phys. A*, Vol. 686, pp. 481-524.

Fassò, A., *et al*. (2001), in *Proceedings of Monte Carlo 2000*, Lisbon, A. Kling, F. Barao, M. Nakagawa, L. Tavora, P. Vaz (eds.), Sprinter-Verlag Berlin, p. 159.

Foucher, Y. (2002), *Étude et développement d'une cible de spallation*, PhD thesis, University of Nantes.

Glasbrenner, H., Y. Dai, F. Gröschel, F. (2005), "LiSoR Irradiation Experiment and Preliminary Post Irradiation Examinations", *Journal of Nuclear Materials*, Vol. 343, pp. 267-274.

Gmelin (1990), *Handbook of Inorganic and Organometallic Chemistry, Polonium*, Supplement Volume 1, Springer-Verlag, Berlin.

Greene, G.A., C.C. Finfrock, http://www.dne.bnl.gov/atd-mag/htm/HgVaporizationJournal.PDF.

Gudowski, W. (2000), "Transmutation of Isotopes – Ecological and Energy Production Aspects", *Acta Physica Polonica B*, Vol. 31, pp. 107-119.

Joy, E.F. (1963), *The Vapour Liquid Equilibrium of Dilute Solutions of Polonium in Liquid Bismuth*, Report MLM-987, Mound Laboratory, Miamisburg, Ohio.

Kirchner, R. (1996), *Nucl. Instrum. Methods B*, Vol. 126, p. 125.

Köster, U. (2000), *Ausbeuten und Spektroskopie Radioaktiver Isotope bei LOHENGRIN und ISOLDE*, PhD thesis, Technische Universität München, and references therein.

Köster, U. (2001), "ISOLDE Target and Ion Source Chemistry", *Radiochim. Acta*, Vol. 89, pp. 749-756.

Krestov, G.A.(1962), *Radiokhimiya*, Vol. 4, p. 690, *Soviet Radiochem.*, Vol. 4, p. 612.

Kugler, E. (2000), "The ISOLDE Facility", *Hyperfine Interactions*, Vol. 129, pp. 23-42.

Langmuir, I. (1913), "The Vapour Pressure of Metallic Tungsten", *Phys. Rev. Second Series*, Vol. 2, pp. 329-342.

Latimer, W.M. (1952), *The Oxidation States of the Elements and Their Potentials in Aqueous Solution*, 2nd ed., Prentice-Hall, Englewood Cliffs, p. 88.

McNeese, L.E. (1967), ORNL-TM-1730, Oak Ridge National Laboratory, Oak Ridge, Tennessee.

Manfrin, E. (2004), private communication.

Mavridis, A., I.K.S. Kerkines (2005), private communication.

Mills, K.C. (1974), *Thermodynamic Data for Inorganic Sulphides, Selenides and Tellurides*, Butterworths, London.

Neuhausen, J., B. Eichler (2003), *Evaluation of Thermochemical Data for Binary Polonium Containing Systems by Means of the Semi-empirical Miedema Model*, PSI-Report Nr. 03-13, September 2003, ISSN 1019-0643.

Neuhausen, J., U. Köster, B. Eichler (2004), "Investigation of Evaporation Characteristics of Polonium and its Lighter Homologues Selenium and Tellurium from Liquid Pb-Bi-eutecticum", *Radiochim. Acta*, Vol. 92, pp. 917-923.

Neuhausen, J., B. Eichler (2005a), "Study of the Thermal Release Behaviour of Mercury and Thallium from Liquid Eutectic Lead-bismuth Alloy", *Radiochimica Acta*, Vol. 93, pp. 155-158.

Neuhausen, J. (2005b), *Reassessment of the Rate of Evaporation of Polonium from Liquid Eutectic Lead Bismuth Alloy*, PSI TM-18-05-01.

Neuhausen, J. (2006), "Investigations on the Release of Mercury from Liquid Eutectic Lead Bismuth Alloy Under Different Gas Atmospheres", *Nucl. Instr. and Meth. A*, forthcoming.

Obara, T., T. Miura, Y. Fujita, Y. Ando, H. Sekimoto (2003), "Preliminary Study of the Removal of Polonium Contamination by Neutron-irradiated Lead-bismuth Eutectic", *Annals of Nucl. Energy*, Vol. 30, pp. 497-502.

Pankratov, D.V., E.I. Efimov, V.N. Bolkovirinov, V.D. Kuranov, M.I. Bugreev (1999), "Polonium Problem in Nuclear Power Plants with Lead-bismuth as a Coolant", in *Heavy Liquid Metal Coolants in Nuclear Technology*, pp. 101-109, Obninsk.

Perret, Ch. (2002), *Sicherheitsbericht zum MEGAPIE-Experiment an einem Target mit flüssigem Blei-Bismut-Eutektikum in der Neutronenquelle SINQ des PSI-West*, PSI, June 2002.

Petrovich, C. (2001), *SP-FISPACT, A Computer Code for Activation and Decay Calculations for Intermediate Energies. A connection of FISPACT and MCNPX*, RT/ERG/2001/10, ENEA, Bologna.

Pitcher, E. (2002), *Summary Report on Neutronics Work in Support of MEGAPIE*, unpublished.

Tupper, R.B., B. Minushkin, Fe.E. Peters, Z.L. Kardos (1991), *Int. Conf. on Fast Reactors and Related Fuel Cycles*, Kyoto, Japan, 28 Oct.-1 Nov. 1991, pp. 5.6-1 to 5.6-9.

Waters, L.S, *et al*., (2002), *MCNPX Users's Manual Version 2.4.0*, LA-CP-02-408.

Zanini, L., M. Vatre (2005), *Monte Carlo Calculations of Activation of the MEGAPIE Target*, PSI report TM-34-05-5.

Zhdanov, S.I. (1985), in: A.J. Bard, R. Parsons, J. Jordan, *Standard Potentials in Aqueous Solution*, Dekker, New York, pp. 93-125.